Hic-5 regulates Src-induced invadopodia rosette formation and organization

Anushree C. Gulvady, Ian J. Forsythe, and Christopher E. Turner*
Department of Cell and Developmental Biology, State University of New York Upstate Medical University, Syracuse, NY 13210

ABSTRACT **Fibroblasts transformed by the proto-oncogene Src form individual invadopodia that can spontaneously self-organize into large matrix-degrading superstructures called rosettes. However, the mechanisms by which the invadopodia can spatiotemporally reorganize their architecture is not well understood. Here, we show that Hic-5, a close relative of the scaffold protein paxillin, is essential for the formation and organization of rosettes in active Src-transfected NIH3T3 fibroblasts and cancer-associated fibroblasts. Live cell imaging, combined with domain-mapping analysis of Hic-5, identified critical motifs as well as phosphorylation sites that are required for the formation and dynamics of rosettes. Using pharmacological inhibition and mutant expression, we show that FAK kinase activity, along with its proximity to and potential interaction with the LD2,3 motifs of Hic-5, is necessary for rosette formation. Invadopodia dynamics and their coalescence into rosettes were also dependent on Rac1, formin, and myosin II activity. Superresolution microscopy revealed the presence of formin FHOD1 and INF2-mediated unbranched radial F-actin fibers emanating from invadopodia and rosettes, which may facilitate rosette formation. Collectively, our data highlight a novel role for Hic-5 in orchestrating the organization of invadopodia into higher-order rosettes, which may promote the localized matrix degradation necessary for tumor cell invasion.**

Monitoring Editor
Alpha Yap
University of Queensland

Received: Oct 10, 2018
Revised: Mar 7, 2019
Accepted: Mar 14, 2019

INTRODUCTION

Invadopodia are specialized F-actin–rich plasma membrane protrusions formed by various cell types within the tumor microenvironment, including tumor cells, cancer-associated fibroblasts (CAFs), and macrophages. These structures are important in the localized secretion of matrix metalloproteinases (MMPs) to proteolytically cleave the surrounding matrix and thereby facilitate tumor cell invasion (Yamaguchi *et al.*, 2006; Schoumacher *et al.*, 2010; Gligorijevic *et al.*, 2012; Weaver *et al.*, 2013; Bergman *et al.*, 2014; Leong *et al.*, 2014; Roh-Johnson *et al.*, 2014; Eddy *et al.*, 2017). Additionally, normal cell types, including dendritic cells and osteoclasts as well as neuronal growth cones, have been studied for their ability to form structures similar to invadopodia (Davies and Stossel, 1977; Caligaris-Cappio *et al.*, 1986; Zambonin-Zallone *et al.*, 1988; Santiago-Medina *et al.*, 2015). Although the invadopodia or invadopodia-like structures formed by each of these various cell types have some differences in structure and molecular composition, they have a common functionality in remodeling the surrounding matrix to facilitate cell-specific functions, including migration through biological barriers, highlighting the need to investigate these structures as potential therapeutic targets (Chen, 1989; Moreau *et al.*, 2003).

Normal fibroblasts expressing a constitutively active form of the nonreceptor tyrosine kinase proto-oncogene c-Src are induced to form both individual invadopodia and organized superstructures of multiple invadopodia called rosettes, with each having matrix degradation abilities that facilitate their transformation into invasive tumorigenic cells (David-Pfeuty and Singer, 1980; Tarone *et al.*, 1985). Interestingly, during normal as well as tumor angiogenesis, vascular endothelial cells have been shown to form rosette-like structures in vivo to remodel the vascular basement membrane and facilitate

This article was published online ahead of print in MBoC in Press (http://www.molbiolcell.org/cgi/doi/10.1091/mbc.E18-10-0629) on March 20, 2019.

*Address correspondence to: C. E. Turner (turnerce@upstate.edu).

Abbreviations used: BSA, bovine serum albumin; CAF, cancer-associated fibroblast; DAPI, 4′6-diamidine-2′-phenylindole; ECM, extracellular matrix; FAK, focal adhesion kinase; FHOD1, formin homology 2 domain containing 1; FITC, fluorescein isothiocyanate; GEF, guanine nucleotide exchange factor; GFP, green fluorescent protein; Hic-5, hydrogen peroxide–inducible clone 5; IgG, immunoglobulin G; INF2, inverted formin-2; KO, knockout; LD, leucine-aspartate; LUT, look-up table; MMP, matrix metalloproteinase; MMTV-PyMT, mouse mammary tumor virus-polyoma middle tumor-antigen; PAK, p21-activated kinase; PDGF, platelet-derived growth factor; PIX, p21-activated kinase-interacting exchange factor; PKL, paxillin kinase linker; PLA, proximity ligation assay; qPCR, quantitative PCR; RNAi, RNA interference; ROCK, Rho kinase; siRes, siRNA resistant; STED, stimulated emission depletion; TGF-β, transforming growth factor β-1; WT, wild type.

blood vessel branching, thus demonstrating the physiological relevance of these structures (Varon *et al.*, 2006; Rottiers *et al.*, 2009; Curado *et al.*, 2014; Seano *et al.*, 2014).

A single mature invadopodium consists of a core containing actin and actin regulators such as cortactin, cofilin, Arp2/3, and N-WASP (DesMarais *et al.*, 2004; Yamaguchi *et al.*, 2005; Artym *et al.*, 2006). In some cell types, the actin core is surrounded by a ring of adhesion proteins including integrins, paxillin, vinculin, alpha-actinin, and Hic-5, as well as Rho-GTPases that tightly regulate invadopodia formation as well as matrix metalloproteinase secretion in a spatiotemporal manner (Bowden *et al.*, 1999; Badowski *et al.*, 2008; Pignatelli *et al.*, 2012). As noted above, the individual invadopodia formed in active Src-transfected fibroblasts can also cluster together and spontaneously reorganize their components into higher-order "rosettes" (David-Pfeuty and Singer, 1980; Tarone *et al.*, 1985; Marchisio *et al.*, 1987; Chen, 1989). These rosettes have the unique advantage of degrading larger areas of underlying extracellular matrix. The formation of invadopodia, their organization into rosettes, and secretion of matrix metalloproteinases, followed by rosette disassembly, is a highly dynamic process occurring over a period of 1–2 h (Pan *et al.*, 2011). Despite their importance, little is known regarding the mechanism(s) that promote the fusion and reorganization of multiple invadopodia into rosettes.

Hic-5 belongs to the paxillin family of focal adhesion–associated proteins (Turner *et al.*, 1990; Turner, 2000a). Hic-5 functions as a molecular scaffold, recruiting an array of structural and signaling components in response to cell–matrix interactions and changes in the extracellular environment to trigger cytoskeletal reorganization (Thomas *et al.*, 1999; Turner, 2000b; Nishiya *et al.*, 2001; Yuminamochi *et al.*, 2003; Hetey *et al.*, 2005; Tumbarello and Turner, 2007; Deakin and Turner, 2011; Deakin *et al.*, 2012b; Pignatelli *et al.*, 2012; Goreczny *et al.*, 2017; Gulvady *et al.*, 2018). Interestingly, ectopic expression of Hic-5 or TGF-β–mediated up-regulation of Hic-5 has been shown to be necessary and sufficient for the formation of matrix-degrading invadopodia in normal breast epithelial MCF10A cells (Pignatelli *et al.*, 2012). In these cells, Hic-5 has been shown to signal via RhoC-ROCK and Rac1-p38MAPK–mediated pathways to regulate invadopodia formation and matrix degradation (Pignatelli *et al.*, 2012). Moreover, Hic-5 has been shown to regulate delivery of membrane-bound type-1 matrix metalloproteinase MT1-MMP to facilitate degradation of the extracellular matrix in active Src-transformed fibroblasts, as well as in endothelial cells to promote angiogenesis (Dave *et al.*, 2016; Petropoulos *et al.*, 2016). Although the functional significance of Hic-5 at the invadopodia has been established, the role of Hic-5 in regulating rosette organization by active Src-transfected fibroblasts has not yet been evaluated.

Here, we provide new mechanistic insight into the mostly unexplored phenomenon of invadopodia coalescence into rosette superstructures, revealing a novel role for Hic-5 in regulating rosette formation and their dynamics in Src-transfected fibroblasts. Our domain-mapping analysis identified key motifs and phosphotyrosine sites utilized by Hic-5 and uncovered crucial functions for the focal adhesion kinase (FAK) and Rac1-GTPase in this Hic-5–mediated rosette assembly. Furthermore, we highlight a potential role for Hic-5 in facilitating formin-mediated radial actin polymerization in promoting coalescence of invadopodia into rosettes.

RESULTS

Hic-5 is required for the formation of rosettes in constitutively active Src-transfected fibroblasts

We have previously demonstrated through TGF-β–mediated up-regulation or ectopic expression of Hic-5 that Hic-5 is necessary and sufficient for the formation of invadopodia in normal breast epithelial MCF10A cells (Pignatelli *et al.*, 2012). To evaluate the requirement for Hic-5 in the formation and function of higher-order rosette structures, we transiently expressed constitutively active Src (Y527F mutant) in the NIH3T3 mouse fibroblast cell line (Roussel *et al.*, 1991; Liu *et al.*, 1993). This nonphosphorylatable mutation at Y527 of Src prevents the autoinhibitory closed conformation of Src, resulting in a highly active kinase (MacAuley and Cooper, 1989; Roussel *et al.*, 1991; Liu *et al.*, 1993). RNA interference (RNAi)-mediated knockdown of Hic-5 with two independent siRNAs in the active Src-expressing fibroblasts resulted in a significant reduction in the ability of these cells to form rosettes (Figure 1, A–C), indicating that Hic-5 is required for rosette formation. However, in contrast to the breast epithelial MCF10A cells (Pignatelli *et al.*, 2012), the Hic-5-depleted active Src fibroblasts retained their ability to form invadopodia, possibly due to cell-specific differences or a residual amount of Hic-5 post siRNA treatment (Figure 1, B and C). In addition, when they were plated on fluorescein isothiocyanate (FITC)-gelatin coated coverslips, no large areas of degradation were observed in the Hic-5-depleted cells, in contrast to the control RNAi-treated fibroblasts expressing active Src (Figure 1, D and E). Although the Hic-5-depleted cells still formed matrix-degrading invadopodia, the activity of these individual invadopodia could not be accurately evaluated due to the presence of the GFP signal within these cells.

We have previously reported the characterization of Hic-5 knockout mouse CAFs that were derived from MMTV-PyMT–induced breast tumors (Goreczny *et al.*, 2017). Active Src was introduced into these primary cells to determine their ability to form invadopodia and rosettes. While the control Hic-5–expressing CAFs did not show any evidence of spontaneously formed invadopodia or rosettes, ectopic expression of active Src stimulated the formation of invadopodia as well as rosettes (Supplemental Figure S1, A and B). In contrast, expression of active Src in the Hic-5 knockout CAFs failed to stimulate any rosette formation. Interestingly, these cells also exhibited reduced numbers of invadopodia in comparison with the control CAFs (Supplemental Figure S1, A and B). This is in contrast to the Hic-5 siRNA-treated active Src expressing NIH3T3 fibroblasts, but similar to the breast epithelial MCF10A cells (Pignatelli *et al.*, 2012), and indicates that Hic-5 is necessary for the formation of both invadopodia and rosettes in the constitutively active Src-expressing mouse CAFs.

Hic-5 localizes to invadopodia and rosettes via the carboxy-terminal LIM domains

Hic-5 contains four amino-terminal leucine aspartate–rich amphipathic helical motifs (LD motifs) within its amino terminus (N-terminus; Tumbarello *et al.*, 2002) that facilitate interactions with various structural and signaling proteins, as well as four carboxy-terminal LIM domains that have previously been shown to facilitate targeting of Hic-5 to focal adhesions (Shibanuma *et al.*, 1994; Brown *et al.*, 1996; Fujita *et al.*, 1998; Matsuya *et al.*, 1998; Thomas *et al.*, 1999; Nishiya *et al.*, 2002; Deakin *et al.*, 2012a; Gulvady *et al.*, 2018). To determine whether the LIM domains are also necessary to target Hic-5 to invadopodia and rosettes, we transiently expressed GFP-Hic-5 WT (full length) and GFP-carboxy terminus (C-terminus), as well as the GFP-N-terminus of Hic-5, in the Y527F Src-expressing NIH3T3 fibroblasts. GFP-Hic-5 WT was enriched in rings around the actin core of individual invadopodia that formed in these cells (Figure 2, A and B, top panel), consistent with the Hic-5–positive rings seen in TGF-β–stimulated MCF10A cells (Pignatelli *et al.*, 2012). The GFP-Hic-5 C-terminus also targeted the invadopodia rings (Figure 2, A and B, middle panel). In contrast, the GFP-Hic-5 N-terminus was unable to

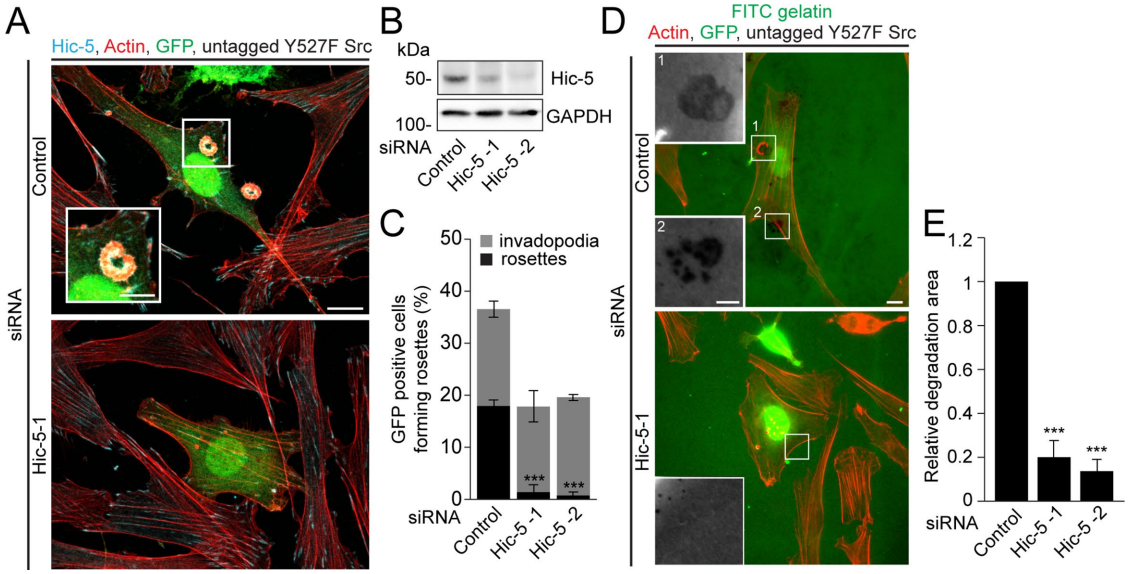

FIGURE 1: Hic-5 is required for formation of rosettes in active Src-transfected NIH3T3 fibroblasts. (A) Representative images of active Src (Y527F mutant)-transfected NIH3T3 fibroblasts after RNAi-mediated knockdown of Hic-5, expressing GFP vector. Scale bar = 10 μm. Inset shows presence of rosettes in the control. Scale bar = 5 μm. (B) Western blot of cell lysates after RNAi-mediated knockdown of Hic-5 using two independent siRNAs in the Y527F Src-transfected NIH3T3 fibroblasts. (C) Quantitation of GFP-positive cells forming either rosettes or invadopodia (n = at least 135 cells). (D) Representative images of cells after RNAi-mediated knockdown of Hic-5, expressing GFP vector and plated on FITC-gelatin matrix. Scale bar = 10 μm. Insets show dark areas of FITC-gelatin degradation. Scale bar = 5 μm. (E) Quantitation of the area of FITC-gelatin degradation per cell area (n = at least 40 cells). Data represent mean ± SEM of at least three independent experiments. A one-way ANOVA with Dunnett's multiple comparison test was performed. ***$p < 0.001$.

target the invadopodia (Figure 2, A and B, bottom panel) or normal focal adhesions found in these cells.

GFP-Hic-5 WT was also observed surrounding the F-actin staining of the more complex rosettes, but demonstrated a gradient of enrichment, with a more robust localization to the inner curvature of the rosette structures (yellow arrowhead) and less localization to their outer surface (Figure 2, C and D, top panel). A similar localization pattern has been reported previously for FAK, paxillin, and Src (Pan *et al.*, 2011; Petropoulos *et al.*, 2016). The GFP-Hic-5 C-terminus had a similar localization to the rosettes (Figure 2, C and D, middle panel), while the GFP-Hic-5 N-terminus was not enriched at these structures (Figure 2, C and D, bottom panel), indicating that the C-terminal LIM domains are required for targeting Hic-5 to individual invadopodia as well as rosettes.

The LD2 and LD3 motifs of Hic-5 are required for the formation and expansion of rosettes

To investigate the domains of Hic-5 and the interacting proteins that mediate rosette formation, we initially expressed Y527F Src, mCherry-Lifeact to visualize the F-actin cytoskeleton, along with GFP-Hic-5 WT or GFP-Hic-5 N-terminus or C-terminus mutants in the fibroblasts, and monitored their effect on rosette formation and dynamics. Time-lapse imaging revealed spontaneous formation of invadopodia with actin cores surrounded by GFP-Hic-5 enriched rings (Figure 3A, top panel, and Supplemental Video S1). Invadopodia were seen to cluster and spontaneously fuse into rosettes within 25–28 min (Figure 3A, top panel). The coalescence was associated with an increase in the F-actin intensity, along with redistribution of Hic-5 from a uniform ring around the F-actin core of invadopodia to a gradient of Hic-5 at the rosettes, with an enriched inner ring and a less bright outer ring of Hic-5 as noted earlier (Figure 3A, top panel). The newly formed rosettes were seen to expand in size and then rapidly disassemble taking an average of 4–5 min. Strikingly, the rapid rosette disassembly was frequently coupled with localized, dynamic bursts of lamellipodia extension and the formation of Hic-5-containing nascent focal adhesions within these lamellipodia (Supplemental Figure S2A, yellow arrows, and Supplemental Video S1). Quantitation of the lifetime of these dynamic rosettes indicated that the process from invadopodia initiation to coalescence into rosettes followed by rapid disassembly lasted on the average 30–40 min (Figure 3C). Interestingly, cells expressing the C-terminus of Hic-5, in contrast to the N-terminus, had a significantly reduced ability to form rosettes, as well as a reduced ability to degrade the underlying FITC gelatin matrix, as compared with the GFP-Hic-5 WT expressing cells (Figure 3, B and D, and Supplemental Figure S2B), indicating that the N-terminus is important in the formation of rosettes.

To determine which, if any, of the key amino-terminal LD motifs of Hic-5 are required for rosette formation, we expressed Y527F Src, mCherry-Lifeact along with GFP-Hic-5 ΔLD1 or ΔLD2, ΔLD3, or ΔLD2,3 mutants in the fibroblasts. Cells expressing each of these mutants were able to form individual invadopodia with the GFP-Hic-5 LD deletion mutants each localizing to the invadopodia ring surrounding the F-actin core (Supplemental Figure S2, B and C). However, GFP-Hic-5 ΔLD2-, ΔLD3-, or ΔLD2,3-, but not ΔLD1-containing invadopodia exhibited a significant defect in the ability to coalescence into rosettes (Figure 3, A, bottom panel, and B, and Supplemental Figure S2B). Additionally, GFP-Hic-5 ΔLD2,3 cells formed invadopodia that were highly stable, with an average lifetime of 50 min, and appeared to exist as loosely connected clusters, as opposed to the robust tightly juxtaposed F-actin cores of the wild type rosettes (Figure 3, A, bottom panel, and C). Nevertheless, these invadopodia retained the ability to degrade the gelatin matrix, although the net area of degradation by the GFP-Hic-5 ΔLD2, ΔLD3,

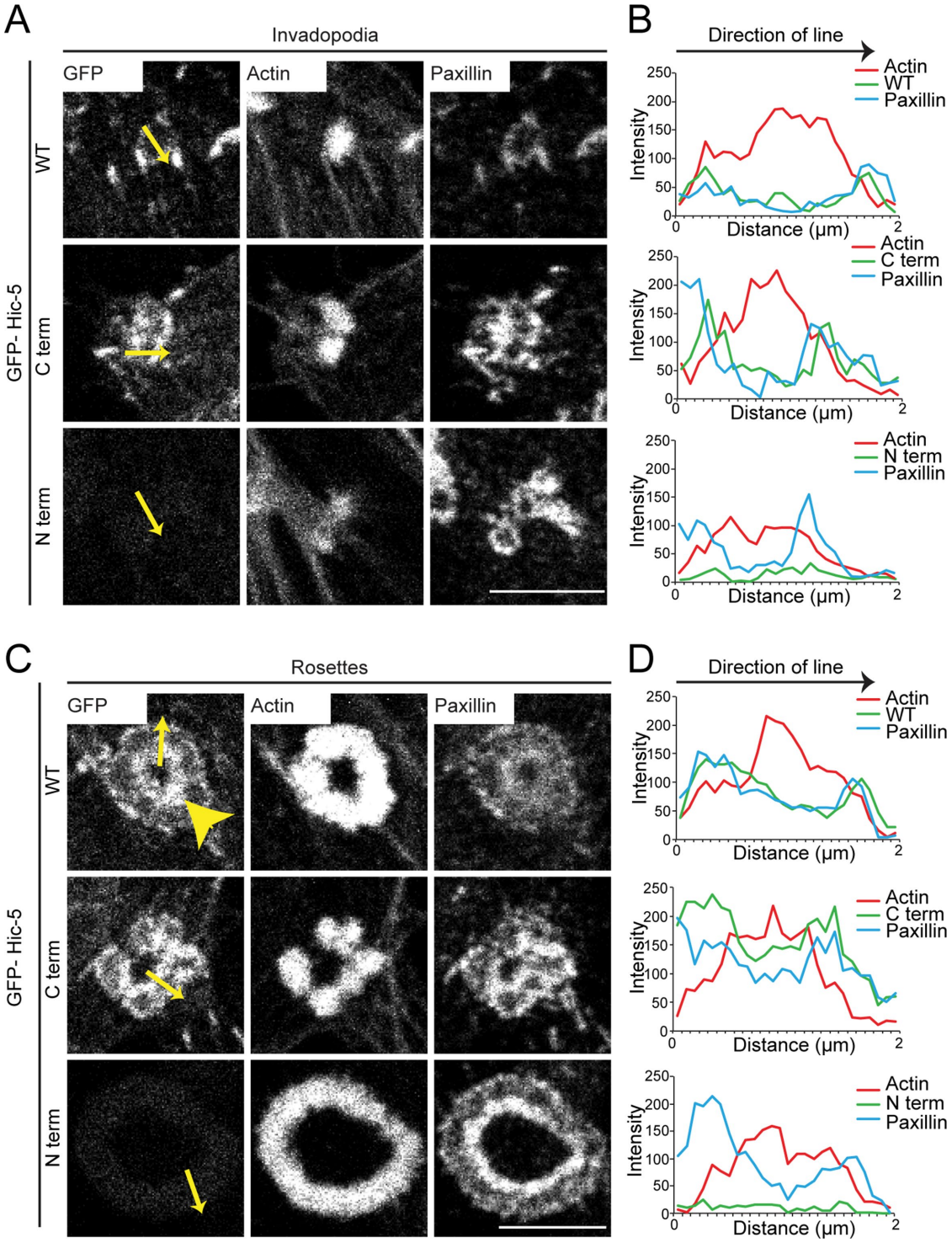

FIGURE 2: Hic-5 localizes to invadopodia and rosettes via the C-terminal LIM domains. Representative images of (A) invadopodia and (C) rosettes formed by active Src-transfected NIH3T3 fibroblasts expressing GFP-Hic-5 WT, C-terminus, or the N-terminus of Hic-5. Scale bar = 5 μm. Line profiles drawn across (B) invadopodia and (D) rosettes show intensities of actin, GFP-Hic-5, and paxillin. Yellow arrows indicate directions of lines drawn for line profiles. Yellow arrowhead indicates an enrichment of Hic-5 at the center of the rosette.

or ΔLD2,3 mutants was lower than with GFP-Hic-5 WT and ΔLD1 mutant-expressing cells (Figure 3D).

Hic-5 contains two well-characterized tyrosine phosphorylation sites, Y38 and Y60, that have been shown previously to be important for Hic-5 function (Fujita *et al.*, 1998; Matsuya *et al.*, 1998; Thomas *et al.*, 1999; Ishino *et al.*, 2000; Hetey *et al.*, 2005; Pignatelli *et al.*, 2012). Interestingly, in contrast to its expression in breast epithelial MCF10A cells (Pignatelli *et al.*, 2012), the nonphosphorylatable Hic-5 Y38,60F mutant–expressing Src-transfected fibroblasts still formed Hic-5 Y38,60F-containing invadopodia (Supplemental Figure S2, B

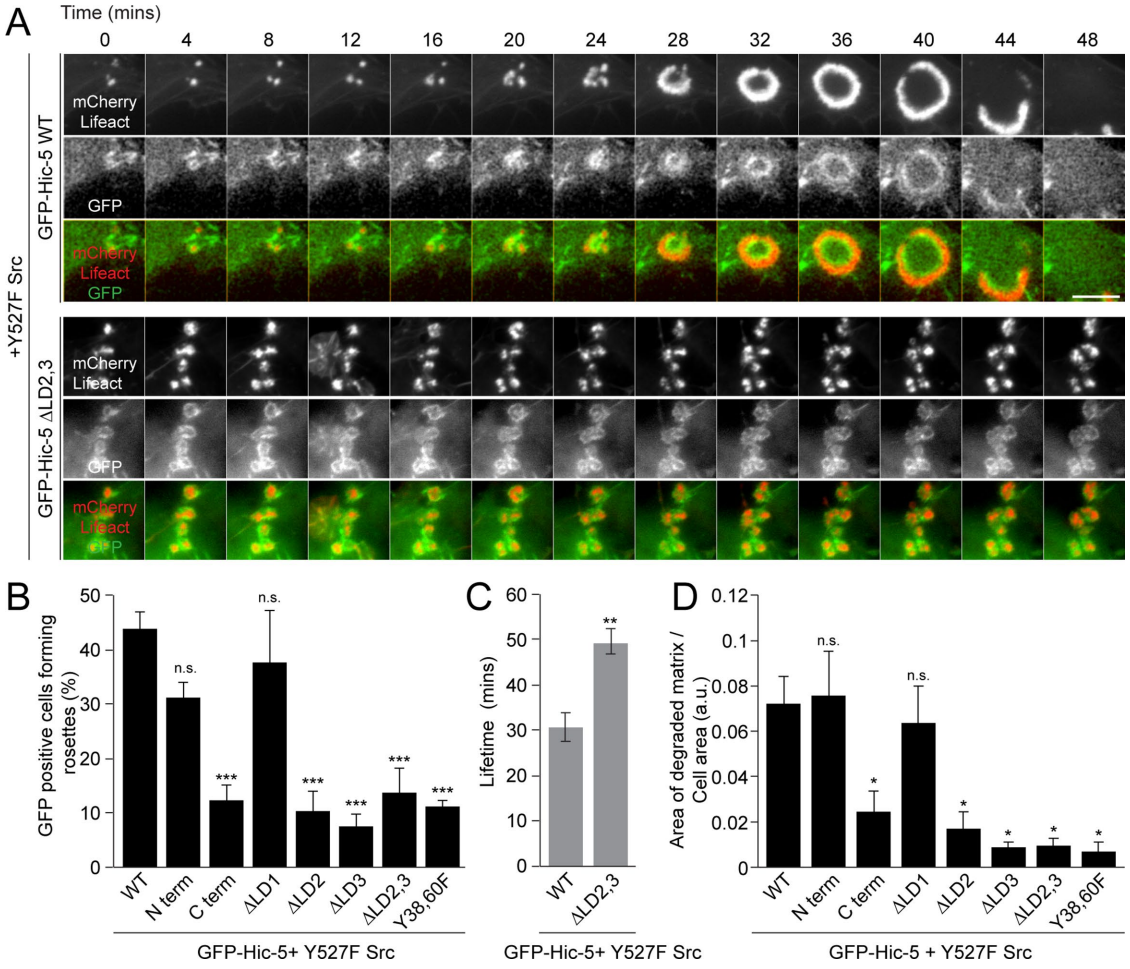

FIGURE 3: The Hic-5 N-terminal LD2 and LD3 motifs, as well as the Y38,60 phosphorylation sites, are required for rosette formation. (A) Time-lapse images of rosette formation in Y527F Src-transfected NIH3T3 fibroblasts expressing mCherry-Lifeact along with GFP-Hic-5 WT or ΔLD2,3 deletion mutant. Scale bar = 5 μm. (B) Quantitation of rosette formation in cells expressing GFP-Hic-5 WT, Hic-5 N-terminus, or C-terminus or ΔLD1, ΔLD2, ΔLD3, ΔLD2,3, or Y38,60F mutants of Hic-5 (n = at least 90 cells). A one-way ANOVA with Dunnett's multiple comparison test was performed. (C) Quantitation of the lifetime of rosettes or invadopodia clusters in cells expressing either GFP-Hic-5 WT or ΔLD2,3 mutant (n = at least 15 cells). An unpaired Student's t test was performed. (D) Quantitation of the area of matrix degraded per cell area, by cells expressing GFP-Hic-5 WT, Hic-5 N-terminus, or C-terminus or ΔLD1, ΔLD2, ΔLD3, ΔLD2,3, or Y38,60F mutants of Hic-5 (n = at least 40 cells). A one-way ANOVA with Dunnett's multiple comparison test was performed. Data represent mean ± SEM of at least three independent experiments. *$p < 0.05$, **$p < 0.01$, and ***$p < 0.001$.

and C), but as was the case with the LD2 and LD3 deletion mutants, the ability of these invadopodia to fuse into rosettes was significantly reduced (Figure 3B and Supplemental Figure S2B), along with the ability to degrade the underlying gelatin matrix (Figure 3D). Taken together, these data indicate that the Hic-5 LD2 and LD3 motifs, along with the Y38,60 phosphorylation sites of Hic-5, are required for the coalescence of individual invadopodia into rosettes.

To evaluate the requirement for Hic-5 WT and the importance of the Hic-5 LD2,3 motifs in rosette formation in the absence of endogenous Hic-5, we repeated the analysis using Y527F Src-transfected NIH3T3 fibroblasts depleted in Hic-5 by RNAi-mediated knockdown and accompanied by transient expression of a GFP-Hic-5 mutant that is resistant to the Hic-5 siRNA (GFP-Hic-5 siRes; Supplemental Figure S3, A and B). The Hic-5 KO CAFs could not be used due to inefficient transfection. Expression of the GFP-Hic-5 siRes in the Hic-5-depleted cells induced a significant increase in their ability to form rosettes over GFP expression (Supplemental Figure S3, B and C), highlighting the requirement for Hic-5 in rosette formation and consistent with our initial analyses (Figure 1). Importantly, as in control cells expressing endogenous Hic-5, rosette formation was severely compromised when the Hic-5 ΔLD2,3 mutant, which is also RNAi-resistant, was expressed in Hic-5-depleted cells (Supplemental Figure S3, B and C). These data further demonstrate a critical role for the Hic-5 LD2,3 motifs in rosette formation in the active Src-expressing NIH3T3 fibroblasts and show that this mutant functions as a dominant negative for rosette formation in cells expressing endogenous Hic-5.

The kinase activity of FAK along with interaction with Hic-5 is necessary for rosette formation

The Hic-5 LD2 and LD3 motifs are homologous to the paxillin LD2 and LD4 motifs, and both pairs of LD motifs have been shown to interact directly with FAK (Bellis *et al.*, 1995; Fujita *et al.*, 1998; Thomas *et al.*, 1999; Bertolucci *et al.*, 2005). Additionally, FAK has

previously been implicated in invadopodia formation in fibroblasts and breast cancer cells (Chan *et al.*, 2009; Pan *et al.*, 2011; Genna *et al.*, 2018). Therefore, we evaluated the requirement for FAK in rosette formation in the Y527F Src–expressing NIH3T3 fibroblasts by inhibiting kinase activity of FAK. Time-lapse imaging indicated that inhibition of FAK activity using the pharmacological inhibitor PF-573228 resulted in almost instantaneous disassembly of existing rosettes and prevented the formation of newer rosettes (Figure 4, A and B, and Supplemental Video S3). Conversely, inhibition of FAK activity did not prevent formation of new invadopodia clusters, as shown previously in fibroblasts and breast cancer cells (Chan *et al.*, 2009; Pan *et al.*, 2011; Genna *et al.*, 2018). However, quantitation of the lifetime of invadopodia clusters in these FAK-inhibited cells indicated that they were highly stable, with an average lifetime of 70–80 min (Figure 4, C and D), phenocopying the Hic-5 ΔLD2,3 mutant (Figure 3C). We also inhibited FAK activity through expression of FAK with a mutation in its kinase domain (K454R), which prevents FAK kinase activity and consequently association with Src (Frisch *et al.*, 1996), and this also resulted in significantly inhibited rosette formation (Figure 4, E and F), confirming that FAK kinase activity is not required for invadopodia formation but is crucial for the formation of higher-order rosettes. To investigate whether a constitutively active form of FAK with enhanced catalytic activity could rescue the coalescence defect seen in the Hic-5 ΔLD2,3–expressing cells, we transiently expressed HA-SuperFAK (K578/581E FAK; Brown *et al.*, 2005), along with the GFP-Hic-5 ΔLD2,3 mutant, in the fibroblasts and found that any invadopodia that formed in these cells still failed to coalesce into rosettes (Figure 4, G and H), implicating FAK activity upstream of the Hic-5–driven signaling pathway during rosette formation. To assess the activity of FAK at the invadopodia formed by cells expressing the GFP-Hic-5 ΔLD3 mutant, we stained the cells for pY397FAK, a readout of FAK autophosphorylation (Schaller *et al.*, 1994). In cells expressing GFP-Hic-5 WT, pY397FAK localized to the rosettes and formed a gradient of pY397FAK enrichment (Figure 5, A and B, and Supplemental Figure S4A), comparable to the localization pattern of Hic-5 (Figure 2C). Interestingly, in cells expressing the GFP-Hic-5 ΔLD3 mutant, pY397FAK still localized to the ring around the actin core of individual invadopodia (Figure 5, A and B, and Supplemental Figure S4A), indicating that FAK localization and activity were unperturbed at the invadopodia that were unable to fuse into rosettes. To assess the ability of FAK to phosphorylate Hic-5, we performed a GFP immunoprecipitation assay using cells expressing GFP-Hic-5 WT treated with or without the FAK inhibitor and analyzed the levels of Hic-5 tyrosine phosphorylation (Supplemental Figure S4B). Following inhibition of the FAK activity, there was a modest, but not statistically significant reduction in the phosphotyrosine levels of Hic-5 (Supplemental Figure S4, B and C), possibly due to the high levels of active Src in these cells. Nevertheless, taken together, these data support a role for the FAK/Src complex upstream of Hic-5 in regulating rosette formation.

We next used an in situ proximity ligation assay (PLA) to test whether FAK and Hic-5 needed to be in close proximity to facilitate invadopodia coalescence into rosettes. A PLA was performed between pY397FAK and GFP in cells expressing GFP-Hic-5 WT or GFP-Hic-5 ΔLD3. In cells expressing GFP-Hic-5 WT, numerous PLA-positive spots were observed at the rosettes as well as focal adhesions, indicative of proximity and a potential interaction between pY397FAK and Hic-5 WT (Figure 5, C and D). In contrast, in cells expressing the GFP-Hic-5 ΔLD3 mutant the number of PLA-positive spots was significantly lower at invadopodia, as well as at focal adhesions (Figure 5, C and D). These data indicate that FAK and Hic-5 are in proximity at the rosettes, and a potential interaction involving the Hic-5 LD3 motif is essential for Hic-5–mediated coalescence of invadopodia into rosettes. To investigate the proximity and potential interaction of FAK with paxillin in these cells, we performed a similar PLA analysis between pY397FAK and paxillin (Figure 5E and Supplemental Figure S4D). Strikingly, numerous positive PLA-spots between pY397FAK and paxillin were observed at the invadopodia and focal adhesions in cells expressing GFP-Hic-5 WT as well as the GFP-Hic-5 ΔLD3 mutant, highlighting that although FAK is in proximity to paxillin, a close relative of Hic-5, the coalescence of rosettes is dependent on the proximity/interaction between FAK and Hic-5.

Rac1 but not ROCK-dependent RhoA signaling is required for rosette organization

Previous studies have indicated a role for the Rho-GTPase Rac1 in mediating invadopodia formation downstream of Hic-5 in the breast epithelial MCF10A cells (Pignatelli *et al.*, 2012). However, Rac1 has also been shown to be required for invadopodia disassembly in MTnL3 cancer cells (Moshfegh *et al.*, 2014). Therefore, to investigate whether Rac1 activity is required for invadopodia and rosette formation in the active Src-transfected NIH3T3 fibroblasts, we inhibited Rac1 pharmacologically using the inhibitor NSC23766 in cells expressing GFP-Hic-5 WT and mCherry-Lifeact. Time-lapse imaging indicated that while Rac1 inhibition did not instantaneously affect the ability of these cells to form invadopodia, Rac1 inhibition induced disassembly of preexisting rosettes and prevented the formation of new rosettes (Figure 6, A and C, and Supplemental Video S4). Furthermore, Rac1-inhibited cells formed stable invadopodia clusters in comparison with control-treated cells, with an average lifetime of 55 min (Figure 6, D and E), similar to the phenotype seen in GFP-Hic-5ΔLD2,3–expressing cells or following FAK inhibition (Figures 3 and 4), suggesting that Rac1 activity may be functioning downstream of Hic-5 in driving coalescence of invadopodia into rosettes. Attempts to utilize a photoactivatable Rac1 probe to activate Rac1 selectively at the invadopodia clusters formed by the Hic-5 ΔLD2,3 mutant cells to potentially rescue the coalescence phenotype were uninformative. Conversely, inhibition of Rho kinase (ROCK) activity, a downstream effector of RhoA signaling, did not prevent rosette formation and actually caused a modest increase in their number (Figure 6, B and C, and Supplemental Video S5).

Formin-mediated actin polymerization is required for the coalescence of invadopodia into rosettes

Analysis of the actin network of podosomes, which are structures analogous to invadopodia formed in macrophages, dendritic cells and osteoclasts (Linder and Aepfelbacher, 2003; Murphy and Courtneidge, 2011), has previously revealed the existence of unbranched actin fibers interconnecting podosome F-actin cores (Luxenburg *et al.*, 2007; van den Dries *et al.*, 2013). Formation of this unbranched actin network has previously been linked to formin-mediated F-actin polymerization (Panzer *et al.*, 2016). Therefore, we hypothesized that the existence of a similar unbranched actin network interconnecting invadopodia clusters in the active Src-transfected NIH3T3 fibroblasts could facilitate fusion of neighboring invadopodia into rosettes. Accordingly, pharmacologic inhibition with the pan-formin inhibitor SMIFH2 (Rizvi *et al.*, 2009) resulted in a significant reduction in invadopodia fusion into rosettes. Time-lapse imaging of active Src-transfected NIH3T3 fibroblasts expressing mCherry-Lifeact revealed that formin inhibition induced rosette disassembly almost instantaneously and was accompanied by a noticeable reduction in the F-actin intensity at the rosettes (Figure 7A and Supplemental Video S6). Furthermore, in the presence of SMIFH2, new invadopodia still formed but were unable to assemble into rosettes

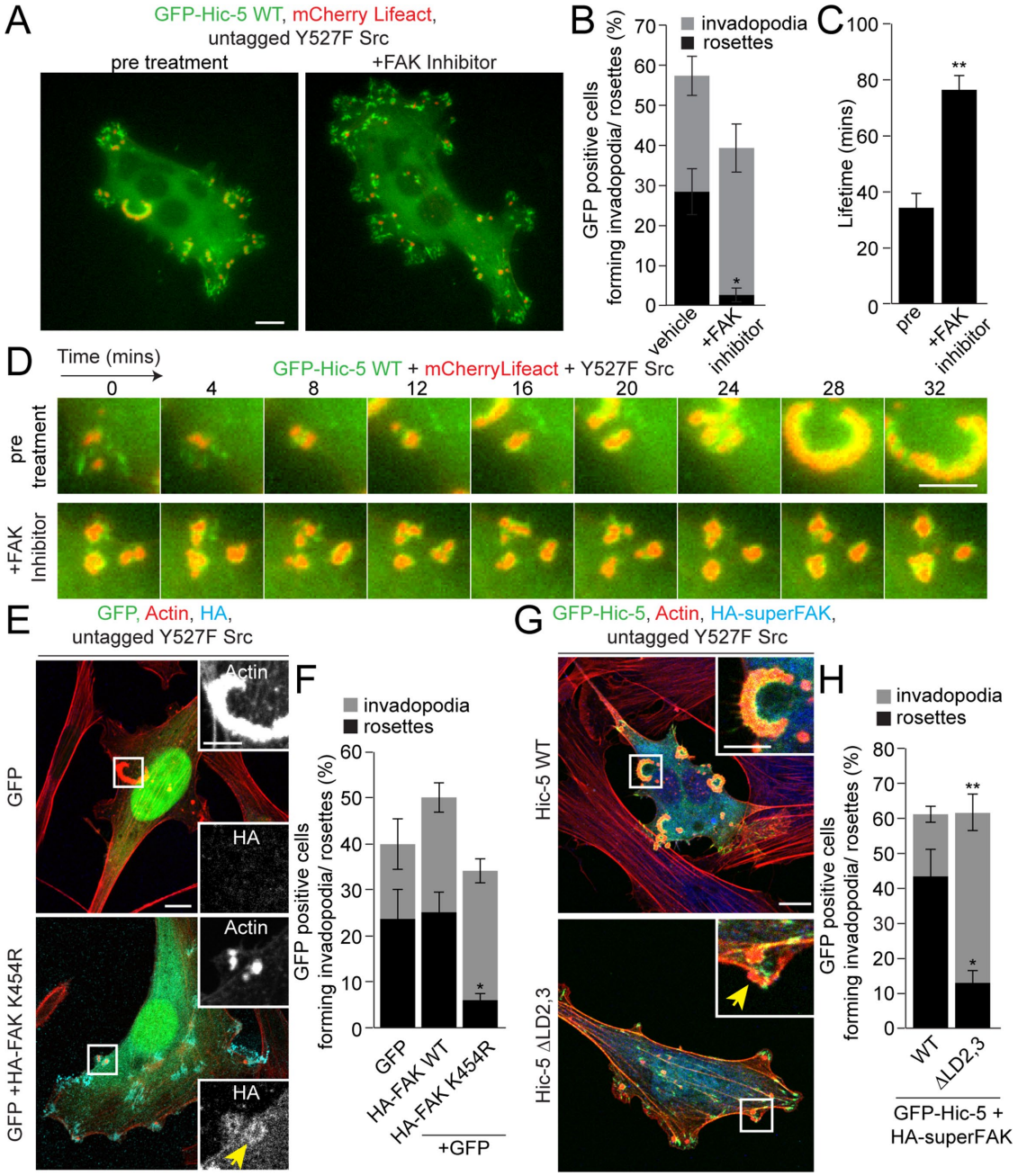

FIGURE 4: The kinase activity of FAK upstream of Hic-5 is required for rosette formation. (A) Representative images of Y527F Src-transfected NIH3T3 fibroblasts expressing GFP-Hic-5 WT and mCherry-Lifeact before and after treatment with the FAK inhibitor PF-573228 (10 μM). Scale bar = 10 μm. (B) Quantitation of cells forming either invadopodia or rosettes after treatment with either vehicle or FAK inhibitor PF-573228 (10 μM) (n = at least 90 cells). (C) Quantitation of the lifetime of rosettes or invadopodia clusters before and after FAK inhibition (n = at least 11 cells). An unpaired Student's t test was performed. (D) Time-lapse images of cells before and after the addition of the FAK inhibitor. Scale bar = 5 μm. (E) Representative images of cells expressing GFP vector or HA-K454R FAK (kinase dead) along with GFP vector and untagged Y527F Src. Scale bar = 10 μm. Insets show actin and HA-FAK staining of the rosettes and invadopodia (yellow arrow). Scale bar = 5 μm. (F) Quantitation of cells forming either individual invadopodia or rosettes (n = at least 85 cells). A one-way ANOVA with Dunnett's multiple comparison test was performed. (G) Representative images of cells expressing GFP-Hic-5 WT or ΔLD2,3 mutant along with HA-superFAK. Scale bar = 10 μm. Insets show higher magnification of invadopodia or rosette (yellow arrow). Scale bar = 5 μm. (H) Quantitation of cells expressing HA-superFAK along with either GFP-Hic-5 WT or ΔLD2,3 mutant and forming either invadopodia or rosettes (n = at least 90 cells). An unpaired Student's t test was performed. Data represent mean ± SEM of at least three independent experiments. *$p < 0.05$ and **$p < 0.01$.

(Figure 7, B and C), similar to the phenotype observed in cells expressing the Hic-5 LD2,3 mutant, as well as following FAK or Rac1 inhibition (Figures 3, 4, and 6). Together, these data suggest a role for formin activity in the polymerization of unbranched radial F-actin fibers in allowing invadopodia to interconnect and subsequently coalesce into rosettes.

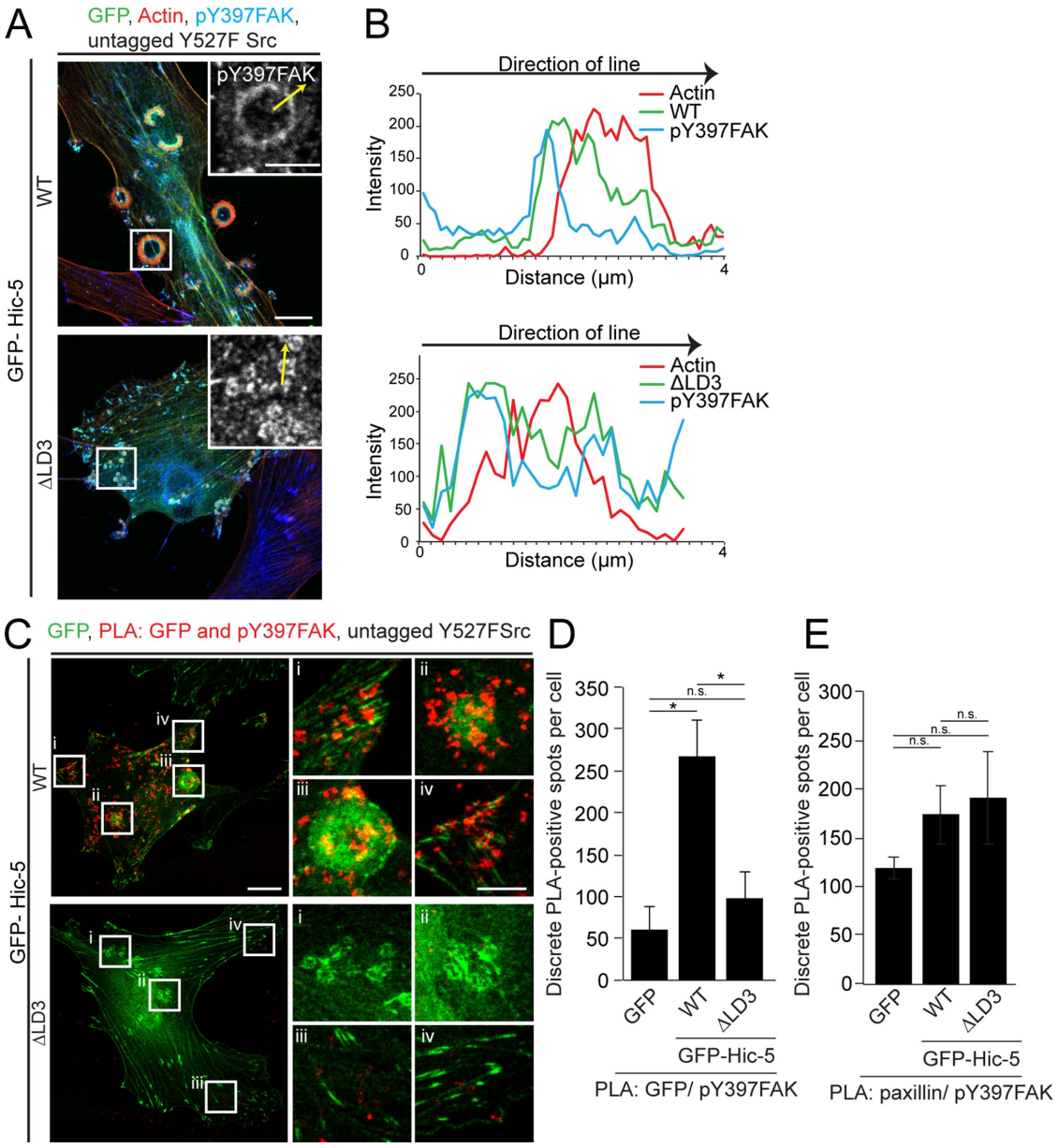

FIGURE 5: Proximity and potential interaction of FAK with Hic-5 LD3 motif is required for rosette formation. (A) Representative images of Y527F Src-transfected NIH3T3 fibroblasts expressing GFP-Hic-5 WT or ΔLD3 mutant stained for pY397FAK. Scale bar = 10 μm. Insets show pY397FAK staining at the rosette and invadopodia. Scale bar = 5 μm. Yellow arrows indicate the directions of the line profiles drawn. (B) Line profiles drawn across the corresponding rosette and an invadopodium show localization of actin, GFP-Hic-5 WT, or ΔLD3 with respect to pY397FAK. (C) Representative images of PLA-positive spots between GFP and pY397FAK in cells expressing GFP-Hic-5 WT or GFP-Hic-5 ΔLD3 mutant. Scale bar = 10 μm. Insets show higher magnification of adhesions, invadopodia, and rosettes. Scale bar = 5 μm. (D) Quantitation of the number of discrete PLA-positive spots between GFP and pY397FAK, seen in GFP control, GFP-Hic-5 WT, or GFP-Hic-5 ΔLD3 mutant expressing cells (n = at least 15 cells). (E) Quantitation of the number of discrete PLA-positive spots between paxillin and pY397FAK, seen in GFP control, GFP-Hic-5 WT, or GFP-Hic-5 ΔLD3 mutant–expressing cells (n = at least 18 cells). Data represent mean ± SEM of at least three independent experiments. A one-way ANOVA with Tukey's multiple comparison test was performed. *$p < 0.05$.

The formins FHOD1 and INF2 have previously been identified as podosome regulators in macrophages (Panzer *et al.*, 2016), potentially downstream of Rac1-GTPase signaling (Gasteier *et al.*, 2003; Schulte *et al.*, 2008; Alvarez and Agaisse, 2013). Additionally, FHOD1 has been implicated in bundling actin fibers that interconnect neighboring podosome cores (Panzer *et al.*, 2016). We therefore investigated the actin polymerization function of the two formins, FHOD1 and INF2, during the process of rosette formation in the active Src-transfected NIH3T3 fibroblasts. Immunofluorescence staining revealed that both FHOD1 and INF2 localize to the actin-rich cores of invadopodia as well as to the rosettes (Figure 7, D and E).

To investigate the functional relevance of these formins in rosette coalescence, we performed an RNAi-mediated knockdown of FHOD1 and INF2 independently, using "smart" pools of multiple siRNAs to the respective formins (Figure 8, A–D; Hannus *et al.*, 2014). Knockdown of either INF2 or FHOD1 significantly

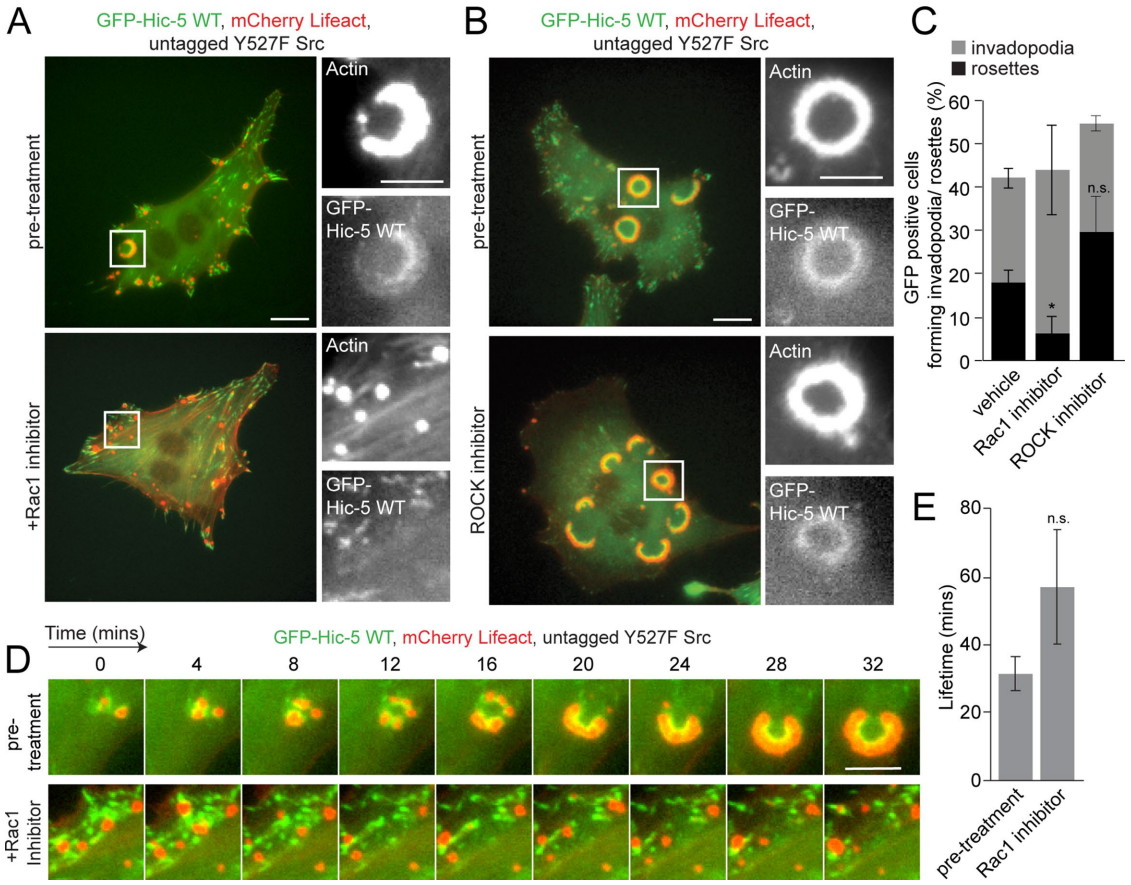

FIGURE 6: Rac1 but not ROCK-dependent RhoA activity is required for rosette organization. (A) Representative images of Y527F Src-transfected fibroblasts expressing GFP-Hic-5 WT along with mCherry-Lifeact, before and after treatment with the Rac1 inhibitor, NSC23766 (100 μM). Scale bar = 10 μm. Insets show higher magnification of the mCherry-Lifeact and GFP-Hic-5 WT-rich invadopodia and rosettes. Scale bar = 5 μm. (B) Representative images of Y527F Src-transfected fibroblasts expressing GFP-Hic-5 WT along with mCherry-Lifeact, before and after treatment with the ROCK inhibitor Y-27632 (10 μM). Scale bar = 10 μm. Insets show higher magnification of the mCherry-Lifeact and GFP-Hic-5 WT-rich rosettes. Scale bar = 5 μm. (C) Quantitation of cells forming either invadopodia or rosettes after Rac1 or ROCK inhibitor treatment (n = at least 90 cells). A one-way ANOVA with a Dunnett's multiple comparison test was performed. (D) Time-lapse imaging before and after Rac1 inhibitor treatment. Scale bar = 5 μm. (E) Quantitation of the lifetime of rosettes or invadopodia clusters before and after Rac1 inhibition. An unpaired Student's t test was performed. Data represent mean ± SEM of at least three independent experiments. *$p < 0.05$.

reduced rosette formation, with a high proportion of cells forming clusters of invadopodia with an inability to coalesce (Figure 8, A and E). Moreover, deconvolved confocal imaging provided evidence of actin fibers extending laterally or outward from the rosettes (Figure 8A inset, white arrows) and also between F-actin hotspots within the rosettes in the control cells (Figure 8A inset, white arrowheads) that were less pronounced in the FHOD1 or INF2 knockdown cells (Figure 8A inset). Superresolution stimulated emission depletion (STED) microscopy analysis of the fibroblasts expressing Hic-5 WT and active Src revealed a similar organization of radial actin fibers arising outward (white arrows) and present within (white arrowheads) organized rosettes (Figure 8F).

Radial actin fibers interconnecting podosomes have previously been shown to be associated with myosin II–driven contractility (Panzer *et al.*, 2016). To test whether rosette formation was also dependent on actomyosin contractility, we inhibited myosin-II activity using a low dose of blebbistatin (5 μM) in cells expressing GFP-Hic-5 WT and mCherry-Lifeact. This treatment resulted in disassembly of rosettes and prevented further coalescence of invadopodia clusters (Supplemental Figure S5), indicating that myosin II–driven contractility is essential in the organization of rosettes, but is independent of ROCK activity (Figure 6). Collectively, these data suggest that Hic-5–mediated regulation of Rac1, along with formin-dependent radial actin fiber assembly and myosin II–driven contractility, plays an important role in facilitating the interconnection of neighboring invadopodia to subsequently promote their coalescence into rosettes (Figure 8G).

DISCUSSION

Proteins involved in invadopodia or invadopodia-like structures have been extensively studied for their contributions to development and disease. Although there are limited reports describing the existence of invadopodia or rosettes in vivo (Hagedorn *et al.*, 2009; Gligorijevic *et al.*, 2012; Seano *et al.*, 2014), there is compelling evidence for deregulation of invadopodia-related proteins in genetic disorders, immune disease, and cancer. Further, expression of established invadopodia components including cortactin, Mena, Tks4, Tks5, MT1-MMP, and Hic-5 has been correlated to poor prognosis of patients with cancers (Shiomi and Okada, 2003; Seals *et al.*, 2005;

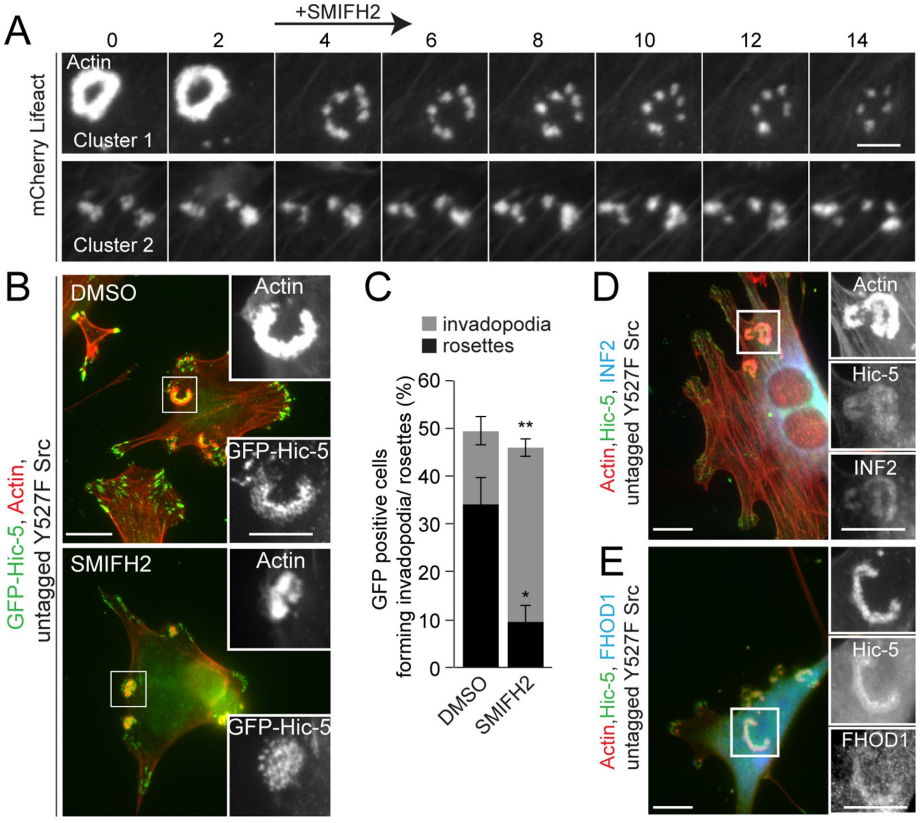

FIGURE 7: Formin activity is required for the coalescence of invadopodia into rosettes. (A) Time-lapse imaging of Y527F Src-transfected cells expressing mCherry-Lifeact treated with a pan-formin inhibitor, SMIFH2 (5 μM). Scale bar = 5 μm. (B) Representative images of cells expressing GFP-Hic-5 WT treated with either DMSO or the formin inhibitor SMIFH2. Scale bar = 10 μm. Insets show higher-magnification images of GFP-Hic-5 and actin staining. Scale bar = 5 μm. (C) Quantitation of cells forming either invadopodia or rosettes before and after treatment with the formin inhibitor (n = at least 90 cells). An unpaired Student's t test was performed. Representative images of actin, Hic-5, and formins (D) INF2 or (E) FHOD1 staining of the rosettes. Scale bar = 10 μm. Insets show individual channels of actin, Hic-5, and formins INF2 or FHOD1. Scale bar = 5 μm. Data represent mean ± SEM of at least three independent experiments. *$p < 0.05$ and **$p < 0.01$.

Hic-5 has also been shown to be a critical modulator of the epithelial-to-mesenchymal transition (Tumbarello and Turner, 2007; Sheta *et al.*, 2017), a process associated with cancer progression. Furthermore, using a range of tumor cell lines, Hic-5 expression was shown to correlate with three-dimensional (3D) mesenchymal morphology (Deakin and Turner, 2011; Gulvady *et al.*, 2018), a mode of cancer cell motility that requires matrix metalloproteinase-mediated remodeling of the surrounding stroma (Brooks *et al.*, 1996; Friedl and Wolf, 2003). Moreover, Hic-5–expressing CAFs have been shown to induce stromal matrix remodeling to promote breast tumor progression in the MMTV-PyMT mouse mammary tumor model system (Goreczny *et al.*, 2017, 2018). Collectively, the evidence highlights the significant role of Hic-5 in facilitating matrix remodeling and tumor invasion.

Hic-5 can interact with multiple cytoplasmic structural and signaling proteins to facilitate cytoskeletal remodeling in response to cell–matrix interactions (Brown and Turner, 2004; Tumbarello and Turner, 2007; Deakin *et al.*, 2012b). Hic-5 is composed of multiple N-terminal LD motifs and C-terminal LIM domains to accommodate these interactions (Shibanuma *et al.*, 1994; Nishiya *et al.*, 1999; Thomas *et al.*, 1999). Our domain-mapping analysis identified a central role for the Hic-5 LIM domains in targeting to invadopodia and rosettes (Figure 2), consistent with their role in focal adhesion targeting (Nishiya *et al.*, 1999). Importantly, the N-terminal LD2 and LD3 motifs of Hic-5 were found to be essential in promoting invadopodia coalescence and rosette formation (Figure 3 and Supplemental Figure S2), as transient expression of the Hic-5 ΔLD2,3 mutant prevented fusion of invadopodia clusters into rosettes. Additionally, these clusters had longer lifetimes, albeit with an inability to fuse into larger rosettes (Figure 3), suggesting an important role for Hic-5 in promoting their disassembly. While our study in NIH3T3 fibroblasts and Hic-5 KO CAFs indicates that paxillin is not sufficient to promote rosette assembly in the absence of Hic-5, this may not be a universal mechanism, since a similar structure–function analysis of paxillin in active Src-transformed paxillin–/– fibroblasts revealed a requirement for all LD motifs of paxillin in coordinating rosette formation, but only after depletion of Hic-5 (Petropoulos *et al.*, 2016), indicating a critical role for Hic-5 in rosette formation and highlighting the complex interplay between paxillin and Hic-5, which may be cell- and context-specific. Importantly, Petropoulos *et al.* (2016) did not examine the mechanism controlling invadopodia cohesion into rosettes, the focus of the current study.

Clark *et al.*, 2007; Weidmann *et al.*, 2016; Goreczny *et al.*, 2018). Given the strong association with human disease, there is a pressing need to understand the underlying mechanisms of invadopodia formation, organization, and matrix degradation.

In the current study, we investigated the function of the focal adhesion adaptor Hic-5 in regulating the formation of invasive rosettes, composed of organized clusters of individual invadopodia. Using constitutively active Src (Y527F)-transfected NIH3T3 fibroblasts or primary CAFs derived from Hic-5 knockout mice (Goreczny *et al.*, 2017), we determined that Hic-5 is necessary for formation of active Src-induced matrix-degrading rosette structures in these cells (Figure 1 and Supplemental Figure S1). The role of Hic-5 in facilitating the function of other matrix degrading structures is well established. For example, TGF-β–induced up-regulation of Hic-5 or ectopic expression of Hic-5 in the human mammary epithelial cell line MCF10A has been shown to be necessary and sufficient for invadopodia formation and matrix degradation (Pignatelli *et al.*, 2012). Moreover, Hic-5 has been found to bridge FAK to MT1-MMP (Dave *et al.*, 2016) and in a separate study also linked to delivering MT1-MMP at the invadopodia site to facilitate degradation of the matrix (Petropoulos *et al.*, 2016).

The focal adhesion kinase (FAK) has been shown to interact with Hic-5 via the LD2 and LD3 motifs (Bellis *et al.*, 1995; Fujita *et al.*, 1998; Thomas *et al.*, 1999; Bertolucci *et al.*, 2005), and using PLA, we have demonstrated that FAK and Hic-5 are maintained in close proximity via the Hic-5 LD3 motif in invadopodia and rosettes (Figure 5). By using a pharmacological inhibitor of FAK, as well as overexpression

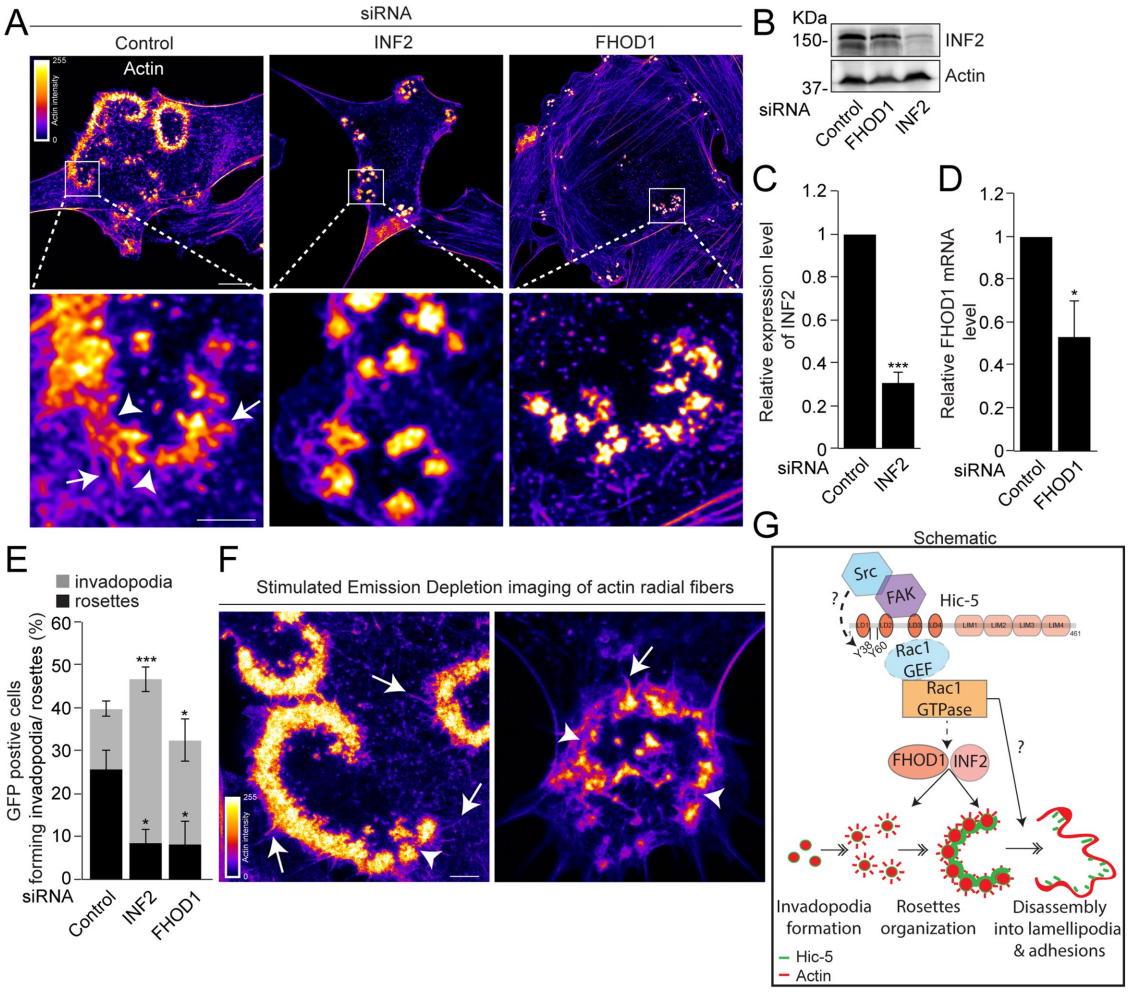

FIGURE 8: FHOD1- and INF2-mediated radial actin polymerization is necessary for coalescence of invadopodia clusters into rosettes. (A) Representative actin- stained, deconvolved, confocal images of Y527F Src-transfected NIH3T3 fibroblasts after RNAi-mediated knockdown of the formins INF2 or FHOD1. Pseudocolored look-up table (LUT) highlights changes in the actin intensity. Scale bar = 10 μm. Insets show presence of F-actin-labeled rosettes in the control and clusters of invadopodia in cells deficient in INF2 or FHOD1 expression. Scale bar = 2.5 μm. White arrows point to radial actin fibers emanating outward from the rosettes. White arrowheads point to radial actin fibers seen within rosettes. (B) Western blot of cell lysates after RNAi-mediated knockdown of INF2. (C) Quantitation of the relative expression of INF2 after RNAi-mediated knockdown of INF2 by Western blot. (D) Quantitation of the mRNA levels of FHOD1 after RNAi-mediated knockdown of FHOD1 as measured by qPCR. An unpaired Student's *t* test was performed. (E) Quantitation of the GFP-positive cells forming either invadopodia or rosettes after RNAi-mediated knockdown (n = at least 90 cells). A one-way ANOVA with a Dunnett's multiple comparison test was performed. (F) Stimulated emission depletion (STED) imaging of F-actin-stained rosettes formed by GFP-Hic-5 WT and Y527F Src-transfected cells. Pseudocolored look-up table (LUT) highlights changes in actin intensity. White arrows point to radial actin fibers emanating outward from the rosettes. White arrowheads point to radial actin fibers seen within the rosettes. Scale bar = 2.5 μm. Data represent mean ± SEM of at least three independent experiments. *$p < 0.05$ and ***$p < 0.001$. (G) Schematic depicting putative model for Hic-5 regulation of rosette formation. Hic-5 interaction with or close proximity to the active FAK-Src complex requiring the Hic-5 LD3 motif is associated with phosphorylation of Hic-5 at Y38,60 sites. Hic-5–dependent stimulation of Rac1 activity, potentially through recruitment of a Rac1GEF to the LD3 motif of Hic-5, along with Rac1-activated FHOD1 and INF2-mediated radial actin polymerization potentially regulates the fusion of invadopodia clusters into rosettes. Rac1 also drives rosette disassembly, which is coordinated with localized lamellipodia extension and potentially directed invasive migration.

of a FAK kinase dead mutant, we determined that FAK kinase activity is also essential for the coalescence of invadopodia into rosettes (Figure 4). FAK has been reported previously to play a dual role in the assembly of "podosome rosettes" in osteoclasts and fibroblasts, through suppression of Rho-mediated vimentin polymerization and p130Cas phosphorylation (Pan *et al.*, 2011). Our data reveal a new function for FAK via its interaction with Hic-5 in driving coalescence and organization of individual invadopodia into rosettes (Figure 4). Moreover, the failure of constitutively active FAK to rescue rosette formation in cells expressing Hic-5 ΔLD2,3 mutant places FAK upstream of Hic-5 in the signaling axis (Figure 4). Interestingly, we observed positive PLA between FAK and paxillin, even in cells exhibiting a defect in invadopodia coalescence caused by expression of Hic-5 ΔLD3 (Figure 5 and Supplemental Figure S4). These data

further highlight the specific role of Hic-5 and the Hic-5-FAK signaling axis in driving rosette assembly.

The domain-mapping analysis also revealed a requirement for phosphorylation of Hic-5 at Y38,60 in invadopodia coalescence into rosettes (Figure 3 and Supplemental Figure S2). Therefore, it is plausible that interaction between the Hic-5 LD3 motif and FAK could promote phosphorylation of Hic-5 via an active FAK/Src complex, and indeed a modest reduction of Hic-5 phosphorylation was observed following FAK inhibition (Supplemental Figure S4B; Hetey *et al.*, 2005). Phosphorylation of Hic-5 at Y38,60 has been shown to be essential during invadopodia formation and matrix degradation in TGF-β–stimulated MCF10A cells as well as in regulating fibronectin fibrillogenesis in CAFs and in driving mesenchymal cell migration in 3D matrices (Fujita *et al.*, 1998; Matsuya *et al.*, 1998; Thomas *et al.*, 1999; Ishino *et al.*, 2000; Pignatelli *et al.*, 2012; Goreczny *et al.*, 2018; Gulvady *et al.*, 2018). It is currently unknown how Hic-5 Y38,60 phosphorylation contributes to rosette coalescence, but one possibility is via indirect regulation of localized Rac1 GTPase activity, as observed in PDGF-stimulated membrane ruffling (Hetey *et al.*, 2005). Similar posttranslational modifications on Y31,118 of the closely related paxillin have also been linked to Rac1 signaling (Brown and Turner, 2004).

Rac1 activity has previously been reported to influence invadopodia dynamics (Revach *et al.*, 2016; Goicoechea *et al.*, 2017), essential for invadopodia formation in MCF10A cells (Pignatelli *et al.*, 2012) and for invadopodia disassembly in MTnL3 cells (Moshfegh *et al.*, 2014). Pharmacological inhibition of Rac1 in the active Src-transfected fibroblasts indicated that Rac1 activity, while being dispensable for invadopodia formation, is crucial for Hic-5–driven organization of invadopodia into rosettes (Figure 6). Given that the Hic-5 LD3 motif, like the paxillin LD4 motif, interacts with the PKL-PIX-PAK complex to control Rac1 signaling (Turner *et al.*, 1999; West *et al.*, 2001), we speculate that Hic-5 interaction with a Rac1 GEF such as PIX is critical to this Rac1-dependent rosette assembly. Interestingly, our time-lapse analysis also revealed that rapid rosette disassembly was frequently accompanied by localized, dynamic bursts of lamellipodia and nascent Hic-5–rich focal adhesion formation (Supplemental Figure 2SA and Supplemental Video 1), indicating multiple, tightly coupled functions for active Rac1. Hic-5 is also implicated in facilitating this Rac1-mediated transition, since expression of the Hic-5 ΔLD2,3 mutant increased the lifetime of invadopodia clusters and reduced the formation of new lamellipodia extensions (Figure 3 and Supplemental Video 2). Moreover, many signaling and structural components localized to invadopodia and rosettes are also present in focal adhesions (Flynn *et al.*, 2008; Murphy and Courtneidge, 2011). Therefore, upon rosette disassembly, protein components within the rosettes could efficiently be recycled directly into these juxtaposed nascent adhesions. Interestingly, HT1080 fibrosarcoma cells migrating within 3D matrices have been shown to form numerous Rac1-driven lateral F-actin–rich protrusions containing focalized β_1 integrins along with MT1-MMP (Wolf *et al.*, 2007; Doyle *et al.*, 2015), presumably contributing to directed cell invasion at these sites. Our data thus shed light on a dual function for Hic-5, not only in regulating rosette formation and localized remodeling of the extracellular matrix (ECM), but also in potentially coupling this with subsequent localized membrane protrusive activity and formation of nascent adhesions, necessary to facilitate tumor cell movement into the resulting void created in the ECM.

Previous analysis of the actin network of podosomes presented evidence for the existence of F-actin fibers interconnecting individual podosome cores in macrophages and dendritic cells (Luxenburg *et al.*, 2007; van den Dries *et al.*, 2013; Meddens *et al.*, 2014). These F-actin fibers were found to be dependent on formin activity, with the fibers being enriched in the formin FHOD1 (Panzer *et al.*, 2016). Superresolution STED imaging of the rosettes in the active Src-transfected fibroblasts revealed the presence of similar formin-regulated F-actin bundles arising within, as well as from the edges of rosettes (Figure 8F). The reduced number of these fibers observed following formin inhibition or knockdown (Figure 8A) suggests that fusion of clusters of invadopodia into rosettes may also be facilitated by formin-dependent F-actin assembly. Furthermore, given that the organization of invadopodia into rosettes is mediated by Rac1 activity (Figure 6), a balance in the Rac1/RhoA signaling could regulate local formin-dependent F-actin assembly (Figures 7 and 8) and actomyosin-based contractility, also shown to be important for maintaining rosette integrity (Supplemental Figure S5; Meddens *et al.*, 2016; Panzer *et al.*, 2016). We speculate that the groups of invadopodia that formed upon expression of the Hic-5 ΔLD2,3 mutant, or following FAK or Rac1 inhibition, may not be interconnected via extensive F-actin fibers (Figures 3, 4, and 6). Rac1-driven or FHOD1- or INF2-mediated F-actin assembly would allow these clusters of invadopodia to interconnect to initiate their reorganization into rosettes (Figure 8G). Time-lapse analysis revealed that invadopodia coalescence in Hic-5 WT–expressing cells is associated with a striking increase in F-actin intensity (Figure 3A), which makes resolving the individual actin cores using conventional light microscopy difficult. Nevertheless, evidence from scanning electron microscopy of podosome expansion in osteoclasts has revealed a 10-fold increase in the amount of F-actin and extensive reorganization in the actin architecture (Luxenburg *et al.*, 2007). The drastic increase in actin intensity was attributed to shorter intercore distances and enhanced actin network protrusion from individual cores, as well as an increase in the actin-core height (Luxenburg *et al.*, 2007). A role for Hic-5 in podosome regulation has not been explored. Nevertheless, a similar reorganization in the F-actin architecture is likely to be occurring during Hic-5–dependent invadopodia coalescence into rosettes in the active Src-transfected NIH3T3 fibroblasts.

MATERIALS AND METHODS

Antibodies and reagents

Antibodies used in this paper include mouse anti-Hic-5 (Cat#611165, BD Biosciences, Franklin Lakes, NJ), mouse anti-paxillin (H-114, Cat#D1615, Santa Cruz Biotechnology, Dallas, TX), mouse anti-HA.11 epitope tag (Clone 16B12, Cat#901502, BioLegend, San Diego, CA), rabbit anti-pTyr397FAK (Cat#700255, Invitrogen, Carlsbad, CA), mouse anti-GFP (B-2, Cat#sc-9996, Santa Cruz Biotechnology, Dallas, TX), rabbit anti-INF2 (Cat#20466-I-AP, Proteintech, Rosemont, IL), rabbit anti-FHOD1 (Cat#AP51668PU-N, Ocrigene, Rockville, MD), mouse anti-GAPDH (Cat#60004-I-Ig, Proteintech, Rosemont, IL), mouse anti-actin (clone C4, Cat# MAB1501, Millipore Sigma, Burlington, MA, for Western blotting), and mouse anti-phosphotyrosine (clone 4G10, Cat#05-321, Millipore Sigma, Burlington, MA). Rhodamine phalloidin (Cat# PHDRI, Cytoskeleton, Denver, CO) and 4′6-diamidine-2′-phenyindole (DAPI; Sigma-Aldrich, St. Louis, MO) were used for detecting F-actin cytoskeleton and the nucleus, respectively. DyLight 488, DyLight 550, and DyLight 633 conjugated anti-mouse and anti-rabbit antibodies (Thermo Fisher Scientific, Waltham, MA) were used for all immunofluorescence studies. Goat anti-rabbit immunoglobulin G (IgG) (H+L)-HRP conjugate (Cat#170-6515, Biorad, Hercules, CA) and goat anti-mouse IgG (H+L)- HRP-conjugated antibodies (Cat#170-6516, Biorad, Hercules, CA) were used for Western blotting. The following inhibitors were used for live and fixed imaging; 10 μM of FAK inhibitor PF573228 (Cat #3239, Tocris Bioscience, Minneapolis, MN),

100 μM of Rac1 inhibitor NSC23766 (Cat #553502, Calbiochem MilliporeSigma, Burlington, MA), 10 μM of ROCK inhibitor Y27632 (Cat #SCM075, MilliporeSigma, Burlington, MA), 5 μM formin inhibitor SMIFH2 (Cat #S4826, Sigma-Aldrich, St. Louis, MO), and 5 μM myosin II inhibitor Blebbistatin (EMD Chemicals, San Diego, CA)

Cell culture

NIH 3T3 fibroblasts obtained from the American Type Culture Collection (Manassas, VA) were cultured in DMEM supplemented with 10% (vol/vol) fetal calf serum, 1 mM sodium pyruvate, 1% (vol/vol) penicillin and streptomycin, and 2 mM L-glutamine. The cells were maintained in a 37°C humidified chamber with 5% CO_2. Primary CAFs were collected as previously described (Nguyen-Ngoc *et al.*, 2015; Goreczny *et al.*, 2017). Briefly, tumors were obtained from the Hic-5$^{+/-}$ and Hic-5$^{-/-}$ PyMT mice, minced, and incubated for 30 min at 37°C in a digestion medium (50:50 DMEM: F12, 5% FBS, 5 μg/ml insulin, 50 μg/ml gentamicin, 2 mg/ml collagenase, 2 mg/ml trypsin), centrifuged at 400 × *g* for 10 min, and then incubated with 80 U of DNase. Single-cell CAFs were obtained by differential centrifugation and were maintained in PyMT medium containing 50:50 DMEM:F12, 10% FBS, 2 mM L-glutamine, and 10 I.U. penicillin/10 μg/ml streptomycin at 5% CO_2 and 37°C. All cell lines have recently been authenticated and tested for contamination.

Transfections and RNAi-mediated protein depletion

NIH3T3 fibroblasts were transiently transfected using Lipofectamine LTX (ThermoFisher, Waltham, MA) following the manufacturer's standard protocol. The CAFs were transfected using Lipofectamine3000 (ThermoFisher, Waltham, MA) according to the manufacturer's standard protocol. Cells were spread on fibronectin-coated coverslips or 35-mm glass-bottomed dishes (MatTek, Ashland, MA) for live imaging 24 h posttransfection. For transfections, the following constructs were used: EGFP, full-length (WT) GFP-Hic-5, and the Hic-5 mutants, GFP-Hic-5 N-terminus, GFP-Hic-5 C-terminus, GFP-Hic-5 ΔLD3, GFP-Hic-5 Y38,60F, were generated as described previously (Hetey *et al.*, 2005). Single-deletion ΔLD1, ΔLD2 and double-deletion ΔLD2,3 mutants were generated and subcloned into the EGFP vector. The pLXSH-Y527FSrc construct was kindly provided by Jonathan A. Cooper (Fred Hutchinson Cancer Research Center, Seattle, WA) and the mCherry-Lifeact construct was kindly provided by Mira Krendel (SUNY Upstate Medical University, Syracuse, NY).

For RNAi-mediated protein depletion, cells were transfected with the siRNA oligos using the Lipofectamine RNAiMAX reagent (ThermoFisher, Waltham, MA) following the manufacturer's standard protocol for 72 h before indicated experiments. The RNAi sequences used were as follows: mouse Hic-5-1: 5′-CCCAUCCGACACAAAAUGGTT-3′ and 5′-CCAUUUUGUGUCGGAUGGGTT-3′; mouse Hic-5-2: 5′-CUGGAUAGACUGAUGGCCUUU-3′ and 5′-AGGCCAUCAGUCUAUCCAGUU-3′ and control 5′-ACUCUAUCUGCACGCUGACUU-3′ and 5′-GUCAGCGUGCAGAUAGAGUUU-3′; mouse FHOD1: 5′-CUACAUACCGUGAGCGCAA-3′, 5′-GUAUCGGACUUGUCGGGAA-3′, 5′-UCGCAUGAUUACCGAGACA-3′, and 5′-UGAGAGUGCCCUUCGGUUA-3′; mouse INF2: 5′UCUCAAAGGGGACGAGCAA-3′, 5′-UUCUAGAAGCGGAGCGGAA-3′, 5′-CAUCCAAUGUGGCACGAGA-3′, and 5′-ACAGAUGGCAAAAGCGGAA-3′ and nontargeting control 5′-UGGUUUACAUGUCGACUAA-3′, 5′-UGGUUUACAUGUUGUGUGA-3′, 5′-UGGUUUACAUGUUUUCUGA-3′, and 5′-UGGUUUACAUGUUUUCCUA-3′. 48 h post RNAi treatment, the cells were transfected with pLXSH-Y527FSrc along with GFP vector for 24 h. The cells were then allowed to spread on fibronectin or FITC-gelatin-coated coverslips for 8 h before fixation.

For the siRNA-resistant experiments, we generated two silent mutations within the mouse GFP-Hic-5 WT construct, without impairing Hic-5's function, using the primers 5′-GCCACTCAGGAACTTGATAGGCTGATGGCCTCGCTC-3′ and 3′-GAGCGAGGCCATCAGCCTATCAAGTTCCTGAGTGGC-5′. These base pair changes within this newly generated siRes Hic-5 construct prevent the mouse Hic-5 siRNA oligo from recognizing it. Further, this siRNA oligo (Hic-5-2) targets the LD3 region of Hic-5 and therefore cannot suppress the expression of the GFP-Hic-5 ΔLD2,3 construct.

Immunofluorescence and time-lapse microscopy

Glass coverslips were incubated with 10 μg/ml fibronectin at 4°C for 16 h in PBS. Cells were spread on the coverslips for 8 h, fixed with 4% (wt/vol) paraformaldehyde/1% Triton X-100 in PBS for 15 min at room temperature, quenched with 0.1 M glycine in phosphate-buffered saline (PBS) for 15 min, and blocked with 3% bovine serum albumin (BSA) in PBS for 16 h at 4°C. For INF2 staining, coverslips were incubated using ice-cold methanol for 15mins at –20°C, permeabilized with 1% Triton X-100 in PBS for 5mins at room temperature followed by blocking with 3% bovine serum albumin (BSA) in PBS for 16 h at 4°C. Primary antibody incubation was performed at 37°C for 2 h, followed by incubation with the appropriate DyLight-conjugated secondary antibodies along with rhodamine phalloidin at 37°C for 1 h. Cells were washed twice and stained with DAPI before being mounted on slides. Coverslips were imaged using an SP8 laser scanning confocal microscope (Leica Hyvolution system; Leica Microsystems) with an HPX Plan Apochromat 63×/1.4 NA oil λ BL objective or a Zeiss Axioskop2 plus microscope fitted with a Qimagin ExiBlue charge-coupled device camera with an Apochromat 63×/0.75 NA objective. Deconvolution of the images was done using the Huygens Professional Deconvolution software (Leica Microsystems) For live cell analysis, transfected cells were spread on 10 μg/ml fibronectin–coated 35-mm glass-bottomed dishes for 6–8 h before imaging. Cells were maintained in complete media at 37° C and 5% CO_2 and tracked live using a Nikon EclipseTi microscope with an S Plan Fluor 63×/1.4 NA objective lens. Images were taken every 2 min for 4 h.

Quantitative PCR (qPCR)

The primers used were fhod1 5′-TGTGCCAACTTCCCGGAAC-3′ and 5′-CTCCGGGTCCAGGTAGTATCC-3′ and mouse GAPDH 5′-GTGTTCCTACCCCCAAATGTGT-3′ and 5′-ATTGTCATACCAGGAAATGAGCTT-3′. The qPCR conditions used were 95°C for 2 min followed by 40 cycles of 95°C for 5 s, 58°C for 30 s, and then 95°C for 5 s. The assay was run on a BioRad CRX384 touch real-time PCR detection system using BioRad iQ SYBR Green Supermix (170-8880). The mRNA levels were normalized to GAPDH using the ΔΔCq method.

Gelatin degradation assay

The assay was performed as previously described (Bowden *et al.*, 2001; Pignatelli *et al.*, 2012). Coverslips were sterilized in ethanol and coated with 50 μg/ml poly-L-lysine (Sigma-Aldrich, St. Louis, MO) in PBS for 15 min, washed in PBS, and incubated with 0.5% glutaraldehyde for 15 min. The slips were then coated with 1:40 fluorescent 488 gelatin (Invitrogen, Carlsbad, CA) with 0.2% wt/vol unlabeled gelatin (Sigma-Aldrich, St. Louis, MO) at 37°C for 30 min. Transfected cells were then spread on the fluorescently labeled gelatin slips for 8 h before fixation. Matrix degradation was quantified as area of degraded matrix/cell area using ImageJ software.

Proximity ligation assays

PLAs were performed according to the manufacturer's guidelines using anti-rabbit and anti-mouse Duolink in situ probes along with the

Duolink in situ detection reagents (Sigma-Aldrich, St. Louis, MO). The discrete PLA-positive spots per cell were counted.

Stimulated emission depletion superresolution microscopy

Images were taken using an SP8 gated stimulated emission depletion (STED) microscope (Leica Microsystems) with an HC PL APO CS2 100×NA 1.4 oil objective. The rhodamine phalloidin–stained cells were imaged using the 550-nm wavelength of the white light laser and depleted with a 660-nm STED laser.

Statistical analysis

A Student's *t* test was used to compare two sets of samples and a one-way analysis of variance (ANOVA) with a Dunnett's, Tukey's, or Sidak's multiple comparison test was used to compare more than three sets of samples. Data represent ±SEM of at least three independent experiments. $*p < 0.05$, $**p < 0.01$, and $***p < 0.001$.

ACKNOWLEDGMENTS

We thank the members of the Turner lab for insightful discussions and Theresa Stowell for expert technical assistance. We thank Jonathan A. Cooper (Fred Hutchinson Cancer Research Center, Seattle, WA) for kindly providing the pLXSH-Y527FSrc construct, Mira Krendel for the mCherry-Lifeact construct, and Scott Blystone for kindly providing the formin inhibitor SMIFH2. We also thank Weiyi Xu for help with the qPCR analysis of FHOD1. This work was supported by the National Institutes of Health (RO1 CA163296 and GM047607 to C.E.T.).

REFERENCES

Alvarez DE, Agaisse H (2013). The formin FHOD1 and the small GTPase Rac1 promote vaccinia virus actin-based motility. J Cell Biol 202, 1075–1090.

Artym VV, Zhang Y, Seillier-Moiseiwitsch F, Yamada KM, Mueller SC (2006). Dynamic interactions of cortactin and membrane type 1 matrix metalloproteinase at invadopodia: defining the stages of invadopodia formation and function. Cancer Res 66, 3034–3043.

Badowski C, Pawlak G, Grichine A, Chabadel A, Oddou C, Jurdic P, Pfaff M, Albiges-Rizo C, Block MR (2008). Paxillin phosphorylation controls invadopodia/podosomes spatiotemporal organization. Mol Biol Cell 19, 633–645.

Bellis SL, Miller JT, Turner CE (1995). Characterization of tyrosine phosphorylation of paxillin in vitro by focal adhesion kinase. J Biol Chem 270, 17437–17441.

Bergman A, Condeelis JS, Gligorijevic B (2014). Invadopodia in context. Cell Adh Migr 8, 273–279.

Bertolucci CM, Guibao CD, Zheng J (2005). Structural features of the focal adhesion kinase-paxillin complex give insight into the dynamics of focal adhesion assembly. Protein Sci 14, 644–652.

Bowden ET, Barth M, Thomas D, Glazer RI, Mueller SC (1999). An invasion-related complex of cortactin, paxillin and PKCmu associates with invadopodia at sites of extracellular matrix degradation. Oncogene 18, 4440–4449.

Bowden ET, Coopman PJ, Mueller SC (2001). Invadopodia: unique methods for measurement of extracellular matrix degradation in vitro. Methods Cell Biol 63, 613–627.

Brooks PC, Stromblad S, Sanders LC, Von Schalscha TL, Aimes RT, Stetler-Stevenson WG, Quigley JP, Cheresh DA (1996). Localization of matrix metalloproteinase MMP-2 to the surface of invasive cells by interaction with integrin alpha v beta 3. Cell 85, 683–693.

Brown MC, Cary LA, Jamieson JS, Cooper JA, Turner CE (2005). Src and FAK kinases cooperate to phosphorylate paxillin kinase linker, stimulate its focal adhesion localization, and regulate cell spreading and protrusiveness. Mol Biol Cell 16, 4316–4328.

Brown MC, Perrotta JA, Turner CE (1996). Identification of LIM3 as the principal determinant of paxillin focal adhesion localization and characterization of a novel motif on paxillin directing vinculin and focal adhesion kinase binding. J Cell Biol 135, 1109–1123.

Brown MC, Turner CE (2004). Paxillin: adapting to change. Physiol Rev 84, 1315–1339.

Caligaris-Cappio F, Bergui L, Tesio L, Corbascio G, Tousco F, Marchisio PC (1986). Cytoskeleton organization is aberrantly rearranged in the cells of B chronic lymphocytic leukemia and hairy cell leukemia. Blood 67, 233–239.

Chan KT, Cortesio CL, Huttenlocher A (2009). FAK alters invadopodia and focal adhesion composition and dynamics to regulate breast cancer invasion. J Cell Biol 185, 357–370.

Chen WT (1989). Proteolytic activity of specialized surface protrusions formed at rosette contact sites of transformed cells. J Exp Zool 251, 167–185.

Clark ES, Whigham AS, Yarbrough WG, Weaver AM (2007). Cortactin is an essential regulator of matrix metalloproteinase secretion and extracellular matrix degradation in invadopodia. Cancer Res 67, 4227–4235.

Curado F, Spuul P, Egana I, Rottiers P, Daubon T, Veillat V, Duhamel P, Leclercq A, Gontier E, Genot E (2014). ALK5 and ALK1 play antagonistic roles in transforming growth factor beta-induced podosome formation in aortic endothelial cells. Mol Cell Biol 34, 4389–4403.

Dave JM, Abbey CA, Duran CL, Seo H, Johnson GA, Bayless KJ (2016). Hic-5 mediates the initiation of endothelial sprouting by regulating a key surface metalloproteinase. J Cell Sci 129, 743–756.

David-Pfeuty T, Singer SJ (1980). Altered distributions of the cytoskeletal proteins vinculin and alpha-actinin in cultured fibroblasts transformed by Rous sarcoma virus. Proc Natl Acad Sci USA 77, 6687–6691.

Davies WA, Stossel TP (1977). Peripheral hyaline blebs (podosomes) of macrophages. J Cell Biol 75, 941–955.

Deakin NO, Ballestrem C, Turner CE (2012a). Paxillin and Hic-5 interaction with vinculin is differentially regulated by Rac1 and RhoA. PLoS One 7, e37990.

Deakin NO, Pignatelli J, Turner CE (2012b). Diverse roles for the paxillin family of proteins in cancer. Genes Cancer 3, 362–370.

Deakin NO, Turner CE (2011). Distinct roles for paxillin and Hic-5 in regulating breast cancer cell morphology, invasion, and metastasis. Mol Biol Cell 22, 327–341.

Desmarais V, Macaluso F, Condeelis J, Bailly M (2004). Synergistic interaction between the Arp2/3 complex and cofilin drives stimulated lamellipod extension. J Cell Sci 117, 3499–3510.

Doyle AD, Carvajal N, Jin A, Matsumoto K, Yamada KM (2015). Local 3D matrix microenvironment regulates cell migration through spatiotemporal dynamics of contractility-dependent adhesions. Nat Commun 6, 8720.

Eddy RJ, Weidmann MD, Sharma VP, Condeelis JS (2017). Tumor cell invadopodia: invasive protrusions that orchestrate metastasis. Trends Cell Biol 27, 595–607.

Flynn DC, Cho Y, Vincent D, Cunnick JM (2008). Podosomes and invadopodia: related structures with common protein components that may promote breast cancer cellular invasion. Breast Cancer (Auckl) 2, 17–29.

Friedl P, Wolf K (2003). Tumour-cell invasion and migration: diversity and escape mechanisms. Nat Rev Cancer 3, 362–374.

Frisch SM, Vuori K, Ruoslahti E, Chan-Hui PY (1996). Control of adhesion-dependent cell survival by focal adhesion kinase. J Cell Biol 134, 793–799.

Fujita H, Kamiguchi K, Cho D, Shibanuma M, Morimoto C, Tachibana K (1998). Interaction of Hic-5, a senescence-related protein, with focal adhesion kinase. J Biol Chem 273, 26516–26521.

Gasteier JE, Madrid R, Krautkramer E, Schroder S, Muranyi W, Benichou S, Fackler OT (2003). Activation of the Rac-binding partner FHOD1 induces actin stress fibers via a ROCK-dependent mechanism. J Biol Chem 278, 38902–38912.

Genna A, Lapetina S, Lukic N, Twafra S, Meirson T, Sharma VP, Condeelis JS, Gil-Henn H (2018). Pyk2 and FAK differentially regulate invadopodia formation and function in breast cancer cells. J Cell Biol 217, 375–395.

Gligorijevic B, Wyckoff J, Yamaguchi H, Wang Y, Roussos ET, Condeelis J (2012). N-WASP-mediated invadopodium formation is involved in intravasation and lung metastasis of mammary tumors. J Cell Sci 125, 724–734.

Goicoechea SM, Zinn A, Awadia SS, Snyder K, Garcia-Mata R (2017). A RhoG-mediated signaling pathway that modulates invadopodia dynamics in breast cancer cells. J Cell Sci 130, 1064–1077.

Goreczny GJ, Forsythe IJ, Turner CE (2018). Hic-5 regulates fibrillar adhesion formation to control tumor extracellular matrix remodeling through interaction with tensin1. Oncogene 37, 1699–1713.

Goreczny GJ, Ouderkirk-Pecone JL, Olson EC, Krendel M, Turner CE (2017). Hic-5 remodeling of the stromal matrix promotes breast tumor progression. Oncogene 36, 2693–2703.

Gulvady AC, Dubois F, Deakin NO, Goreczny GJ, Turner CE (2018). Hic-5 expression is a major indicator of cancer cell morphology, migration, and plasticity in three-dimensional matrices. Mol Biol Cell 29, 1704–1717.
Hagedorn EJ, Yashiro H, Ziel JW, Ihara S, Wang Z, Sherwood DR (2009). Integrin acts upstream of netrin signaling to regulate formation of the anchor cell's invasive membrane in C. elegans. Dev Cell 17, 187–98.
Hannus M, Beitzinger M, Engelmann JC, Weickert MT, Spang R, Hannus S, Meister G (2014). siPools: highly complex but accurately defined siRNA pools eliminate off-target effects. Nucleic Acids Res 42, 8049–8061.
Hetey SE, Lalonde DP, Turner CE (2005). Tyrosine-phosphorylated Hic-5 inhibits epidermal growth factor-induced lamellipodia formation. Exp Cell Res 311, 147–156.
Ishino M, Aoto H, Sasaski H, Suzuki R, Sasaki T (2000). Phosphorylation of Hic-5 at tyrosine 60 by CAKbeta and Fyn. FEBS Lett 474, 179–183.
Leong HS, Robertson AE, Stoletov K, Leith SJ, Chin CA, Chien AE, Hague MN, Ablack A, Carmine-Simmen K, McPherson VA, *et al*. (2014). Invadopodia are required for cancer cell extravasation and are a therapeutic target for metastasis. Cell Rep 8, 1558–1570.
Linder S, Aepfelbacher M (2003). Podosomes: adhesion hot-spots of invasive cells. Trends Cell Biol 13, 376–385.
Liu X, Brodeur SR, Gish G, Songyang Z, Cantley LC, Laudano AP, Pawson T (1993). Regulation of c-Src tyrosine kinase activity by the Src SH2 domain. Oncogene 8, 1119–1126.
Luxenburg C, Geblinger D, Klein E, Anderson K, Hanein D, Geiger B, Addadi L (2007). The architecture of the adhesive apparatus of cultured osteoclasts: from podosome formation to sealing zone assembly. PLoS One 2, e179.
MacAuley A, Cooper JA (1989). Structural differences between repressed and derepressed forms of p60c-src. Mol Cell Biol 9, 2648–2656.
Marchisio PC, Cirillo D, Teti A, Zambonin-Zallone A, Tarone G (1987). Rous sarcoma virus-transformed fibroblasts and cells of monocytic origin display a peculiar dot-like organization of cytoskeletal proteins involved in microfilament-membrane interactions. Exp Cell Res 169, 202–214.
Matsuya M, Sasaki H, Aoto H, Mitaka T, Nagura K, Ohba T, Ishino M, Takahashi S, Suzuki R, Sasaki T (1998). Cell adhesion kinase beta forms a complex with a new member, Hic-5, of proteins localized at focal adhesions. J Biol Chem 273, 1003–1014.
Meddens MB, Pandzic E, Slotman JA, Guillet D, Joosten B, Mennens S, Paardekooper LM, Houtsmuller AB, Van Den Dries K, Wiseman PW, Cambi A (2016). Actomyosin-dependent dynamic spatial patterns of cytoskeletal components drive mesoscale podosome organization. Nat Commun 7, 13127.
Meddens MB, Van Den Dries K, Cambi A (2014). Podosomes revealed by advanced bioimaging: what did we learn? Eur J Cell Biol 93, 380–387.
Moreau V, Tatin F, Varon C, Genot E (2003). Actin can reorganize into podosomes in aortic endothelial cells, a process controlled by Cdc42 and RhoA. Mol Cell Biol 23, 6809–6822.
Moshfegh Y, Bravo-Cordero JJ, Miskolci V, Condeelis J, Hodgson L (2014). A Trio-Rac1-Pak1 signalling axis drives invadopodia disassembly. Nat Cell Biol 16, 574–586.
Murphy DA, Courtneidge SA (2011). The "ins" and "outs" of podosomes and invadopodia: characteristics, formation and function. Nat Rev Mol Cell Biol 12, 413–426.
Nguyen-Ngoc KV, Shamir ER, Huebner RJ, Beck JN, Cheung KJ, Ewald AJ (2015). 3D culture assays of murine mammary branching morphogenesis and epithelial invasion. Methods Mol Biol 1189, 135–162.
Nishiya N, Iwabuchi Y, Shibanuma M, Cote JF, Tremblay ML, Nose K (1999). Hic-5, a paxillin homologue, binds to the protein-tyrosine phosphatase PEST (PTP-PEST) through its LIM 3 domain. J Biol Chem 274, 9847–9853.
Nishiya N, Shirai T, Suzuki W, Nose K (2002). Hic-5 interacts with GIT1 with a different binding mode from paxillin. J Biochem 132, 279–289.
Nishiya N, Tachibana K, Shibanuma M, Mashimo JI, Nose K (2001). Hic-5-reduced cell spreading on fibronectin: competitive effects between paxillin and Hic-5 through interaction with focal adhesion kinase. Mol Cell Biol 21, 5332–5345.
Pan YR, Chen CL, Chen HC (2011). FAK is required for the assembly of podosome rosettes. J Cell Biol 195, 113–129.
Panzer L, Trube L, Klose M, Joosten B, Slotman J, Cambi A, Linder S (2016). The formins FHOD1 and INF2 regulate inter- and intra-structural contractility of podosomes. J Cell Sci 129, 298–313.
Petropoulos C, Oddou C, Emadali A, Hiriart-Bryant E, Boyault C, Faurobert E, Vande Pol S, Kim-Kaneyama JR, Kraut A, Coute Y, *et al*. (2016). Roles of paxillin family members in adhesion and ECM degradation coupling at invadosomes. J Cell Biol 213, 585–599.
Pignatelli J, Tumbarello DA, Schmidt RP, Turner CE (2012). Hic-5 promotes invadopodia formation and invasion during TGF-beta-induced epithelial-mesenchymal transition. J Cell Biol 197, 421–437.
Revach OY, Winograd-Katz SE, Samuels Y, Geiger B (2016). The involvement of mutant Rac1 in the formation of invadopodia in cultured melanoma cells. Exp Cell Res 343, 82–88.
Rizvi SA, Neidt EM, Cui J, Feiger Z, Skau CT, Gardel ML, Kozmin SA, Kovar DR (2009). Identification and characterization of a small molecule inhibitor of formin-mediated actin assembly. Chem Biol 16, 1158–1168.
Roh-Johnson M, Bravo-Cordero JJ, Patsialou A, Sharma VP, Guo P, Liu H, Hodgson L, Condeelis J (2014). Macrophage contact induces RhoA GTPase signaling to trigger tumor cell intravasation. Oncogene 33, 4203–4212.
Rottiers P, Saltel F, Daubon T, Chaigne-Delalande B, Tridon V, Billottet C, Reuzeau E, Genot E (2009). TGFbeta-induced endothelial podosomes mediate basement membrane collagen degradation in arterial vessels. J Cell Sci 122, 4311–4318.
Roussel RR, Brodeur SR, Shalloway D, Laudano AP (1991). Selective binding of activated pp60c-src by an immobilized synthetic phosphopeptide modeled on the carboxyl terminus of pp60c-src. Proc Natl Acad Sci USA 88, 10696–10700.
Santiago-Medina M, Gregus KA, Nichol RH, O'toole SM, Gomez TM (2015). Regulation of ECM degradation and axon guidance by growth cone invadosomes. Development 142, 486–496.
Schaller MD, Hildebrand JD, Shannon JD, Fox JW, Vines RR, Parsons JT (1994). Autophosphorylation of the focal adhesion kinase, pp125FAK, directs SH2-dependent binding of pp60src. Mol Cell Biol 14, 1680–1688.
Schoumacher M, Goldman RD, Louvard D, Vignjevic DM (2010). Actin, microtubules, and vimentin intermediate filaments cooperate for elongation of invadopodia. J Cell Biol 189, 541–556.
Schulte A, Stolp B, Schonichen A, Pylypenko O, Rak A, Fackler OT, Geyer M (2008). The human formin FHOD1 contains a bipartite structure of FH3 and GTPase-binding domains required for activation. Structure 16, 1313–1323.
Seals DF, Azucena EF Jr, Pass I, Tesfay L, Gordon R, Woodrow M, Resau JH, Courtneidge SA (2005). The adaptor protein Tks5/Fish is required for podosome formation and function, and for the protease-driven invasion of cancer cells. Cancer Cell 7, 155–165.
Seano G, Chiaverina G, Gagliardi PA, DI Blasio L, Puliafito A, Bouvard C, Sessa R, Tarone G, Sorokin L, Helley D, *et al*. (2014). Endothelial podosome rosettes regulate vascular branching in tumour angiogenesis. Nat Cell Biol 16, 931–941, 1–8.
Sheta R, Wang ZQ, Bachvarova M, Plante M, Gregoire J, Renaud MC, Sebastianelli A, Gobeil S, Morin C, Macdonald E, *et al*. (2017). Hic-5 regulates epithelial to mesenchymal transition in ovarian cancer cells in a TGFbeta1-independent manner. Oncotarget 8, 82506–82530.
Shibanuma M, Mashimo J, Kuroki T, Nose K (1994). Characterization of the TGF beta 1-inducible hic-5 gene that encodes a putative novel zinc finger protein and its possible involvement in cellular senescence. J Biol Chem 269, 26767–26774.
Shiomi T, Okada Y (2003). MT1-MMP and MMP-7 in invasion and metastasis of human cancers. Cancer Metastasis Rev 22, 145–152.
Tarone G, Cirillo D, Giancotti FG, Comoglio PM, Marchisio PC (1985). Rous sarcoma virus-transformed fibroblasts adhere primarily at discrete protrusions of the ventral membrane called podosomes. Exp Cell Res 159, 141–157.
Thomas SM, Hagel M, Turner CE (1999). Characterization of a focal adhesion protein, Hic-5, that shares extensive homology with paxillin. J Cell Sci, 112(Pt 2), 181–190.
Tumbarello DA, Brown MC, Turner CE (2002). The paxillin LD motifs. FEBS Lett 513, 114–118.
Tumbarello DA, Turner CE (2007). Hic-5 contributes to epithelial-mesenchymal transformation through a RhoA/ROCK-dependent pathway. J Cell Physiol 211, 736–747.
Turner CE (2000a). Paxillin and focal adhesion signalling. Nat Cell Biol 2, E231–E236.
Turner CE (2000b). Paxillin interactions. J Cell Sci, 113(Pt 23), 4139–4140.
Turner CE, Brown MC, Perrotta JA, Riedy MC, Nikolopoulos SN, Mcdonald AR, Bagrodia S, Thomas S, Leventhal PS (1999). Paxillin LD4 motif binds PAK and PIX through a novel 95-kD ankyrin repeat, ARF-GAP protein: A role in cytoskeletal remodeling. J Cell Biol 145, 851–863.
Turner CE, Glenney JR Jr, Burridge K (1990). Paxillin: a new vinculin-binding protein present in focal adhesions. J Cell Biol 111, 1059–1068.
van den Dries K, Schwartz SL, Byars J, Meddens MB, Bolomini-Vittori M, Lidke DS, Figdor CG, Lidke KA, Cambi A (2013). Dual-color

superresolution microscopy reveals nanoscale organization of mechanosensory podosomes. Mol Biol Cell 24, 2112–2123.
Varon C, Tatin F, Moreau V, Van Obberghen-Schilling E, Fernandez-Sauze S, Reuzeau E, Kramer I, Genot E (2006). Transforming growth factor beta induces rosettes of podosomes in primary aortic endothelial cells. Mol Cell Biol 26, 3582–3594.
Weaver AM, Page JM, Guelcher SA, Parekh A (2013). Synthetic and tissue-derived models for studying rigidity effects on invadopodia activity. Methods Mol Biol 1046, 171–189.
Weidmann MD, Surve CR, Eddy RJ, Chen X, Gertler FB, Sharma VP, Condeelis JS (2016). Mena(INV) dysregulates cortactin phosphorylation to promote invadopodium maturation. Sci Rep 6, 36142.
West KA, Zhang H, Brown MC, Nikolopoulos SN, Riedy MC, Horwitz AF, Turner CE (2001). The LD4 motif of paxillin regulates cell spreading and motility through an interaction with paxillin kinase linker (PKL). J Cell Biol 154, 161–176.
Wolf K, Wu YI, Liu Y, Geiger J, Tam E, Overall C, Stack MS, Friedl P (2007). Multi-step pericellular proteolysis controls the transition from individual to collective cancer cell invasion. Nat Cell Biol 9, 893–904.
Yamaguchi H, Lorenz M, Kempiak S, Sarmiento C, Coniglio S, Symons M, Segall J, Eddy R, Miki H, Takenawa T, Condeelis J (2005). Molecular mechanisms of invadopodium formation: the role of the N-WASP-Arp2/3 complex pathway and cofilin. J Cell Biol 168, 441–452.
Yamaguchi H, Pixley F, Condeelis J (2006). Invadopodia and podosomes in tumor invasion. Eur J Cell Biol 85, 213–218.
Yuminamochi T, Yatomi Y, Osada M, Ohmori T, Ishii Y, Nakazawa K, Hosogaya S, Ozaki Y (2003). Expression of the LIM proteins paxillin and Hic-5 in human tissues. J Histochem Cytochem 51, 513–521.
Zambonin-Zallone A, Teti A, Carano A, Marchisio PC (1988). The distribution of podosomes in osteoclasts cultured on bone laminae: effect of retinol. J Bone Miner Res 3, 517–523.